PLOS COMPUTATIONAL BIOLOGY

RESEARCH ARTICLE

Bivalent chromatin as a therapeutic target in cancer: An *in silico* predictive approach for combining epigenetic drugs

Tomás Alarcón[1,2,3]*, **Josep Sardanyés**[2], **Antoni Guillamon**[2,4,5], **Javier A. Menendez**[6,7]

1 Institució Catalana de Recerca i Estudis Avançats (ICREA), Barcelona, Spain, **2** Centre de Recerca Matemàtica, Cerdanyola del Vallès, Spain, **3** Departament de Matemàtiques, Universitat Autònoma de Barcelona, Cerdanyola del Vallès, Spain, **4** Departament de Matemàtiques, EPSEB, Universitat Politècnica de Catalunya, Barcelona, Spain, **5** Institut de Matemàtiques de la UPC-BarcelonaTech (IMTech), Universitat Politècnica de Catalunya, Barcelona, Spain, **6** Program Against Cancer Therapeutic Resistance (ProCURE), Metabolism and Cancer Group, Catalan Institute of Oncology, Girona, Spain, **7** Girona Biomedical Research Institute, Salt, Girona, Spain

* talarcon@crm.cat

Citation: Alarcón T, Sardanyés J, Guillamon A, Menendez JA (2021) Bivalent chromatin as a therapeutic target in cancer: An *in silico* predictive approach for combining epigenetic drugs. PLoS Comput Biol 17(6): e1008408. https://doi.org/10.1371/journal.pcbi.1008408

Editor: Ilya Ioshikhes, University of Ottawa, CANADA

Received: October 11, 2020

Accepted: April 26, 2021

Published: June 21, 2021

Data Availability Statement: All relevant data are within the manuscript and its Supporting information files.

Funding: T.A., J.A.M., and J.S. have been partially funded by the CERCA Programme of the Generalitat de Catalunya. The authors also acknowledge support from State Research Agency under grants MTM2015-71509-C2-1-R (T.A. and J. S.), MTM2015-71509-C2-2-R (A.G.), RTI2018-098322-B-I00 (T.A. and J.S.), PGC2018-098676-B-I00 (A.G.), RTI2018-093860-B-C21 (A.G.), and

Abstract

Tumour cell heterogeneity is a major barrier for efficient design of targeted anti-cancer therapies. A diverse distribution of phenotypically distinct tumour-cell subpopulations prior to drug treatment predisposes to non-uniform responses, leading to the elimination of sensitive cancer cells whilst leaving resistant subpopulations unharmed. Few strategies have been proposed for quantifying the variability associated to individual cancer-cell heterogeneity and minimizing its undesirable impact on clinical outcomes. Here, we report a computational approach that allows the rational design of combinatorial therapies involving epigenetic drugs against chromatin modifiers. We have formulated a stochastic model of a bivalent transcription factor that allows us to characterise three different qualitative behaviours, namely: bistable, high- and low-gene expression. Comparison between analytical results and experimental data determined that the so-called bistable and high-gene expression behaviours can be identified with undifferentiated and differentiated cell types, respectively. Since undifferentiated cells with an aberrant self-renewing potential might exhibit a cancer/metastasis-initiating phenotype, we analysed the efficiency of combining epigenetic drugs against the background of heterogeneity within the bistable sub-ensemble. Whereas single-targeted approaches mostly failed to circumvent the therapeutic problems represented by tumour heterogeneity, combinatorial strategies fared much better. Specifically, the more successful combinations were predicted to involve modulators of the histone H3K4 and H3K27 demethylases KDM5 and KDM6A/UTX. Those strategies involving the H3K4 and H3K27 methyltransferases MLL2 and EZH2, however, were predicted to be less effective. Our theoretical framework provides a coherent basis for the development of an *in silico* platform capable of identifying the epigenetic drugs combinations best-suited to therapeutically manage non-uniform responses of heterogenous cancer cell populations.

PID2019-10455GB-I00 (J.M.) and AGAUR projects 2014SGR229 (T.A.) 2017SGR1049, (A.G.) and 2017SGR01735 (T.A. and J.S.). J.S. has been also funded by a "Ramón y Cajal" Fellowship (RYC-2017-22243). The funders had no role in study design, data collection, and analysis, decision to publish, or preparation of the manuscript.

Competing interests: The authors have declared that no competing interests exist.

Author summary

Heterogeneity in cancer cell populations is one of the main engines of resistance to targeted therapies, as it induces nonuniform responses within the population that clears the sensitive subpopulation, whilst leaving unaffected the non-responsive cells. Although this is a well-known fact, few successful approaches have been proposed aimed at both quantifying the variability associated to cell heterogeneity, and characterising strategies that circumvent its drug-resistance inducing effects. Here we present a computational approach that addresses these issues in the particular context of targeting epigenetic regulators (specifically, chromatin modifiers), which have been proposed as therapeutic targets in several types of cancer and also in ageing-related diseases. Our model predicts that the more successful combinations involve modulators of demethylase activity (specifically, KDM5/6 and UTX). By contrast, strategies involving EZH2 activity are predicted to be less effective. Our results support the use of our framework as a platform for *in silico* drug trials, as it accounts for non-homogeneous response of cell populations to drugs as well as identifying which subpopulations are more likely to respond to specific strategies.

Introduction

Heterogeneity is a primary cause of *de novo* and acquired resistance to targeted treatments in cancer therapeutics [1–3]. There is ample evidence of genetic diversity among cancer cells both within and across tumours [4–6], with genomic instability being the main engine of heterogeneity [7]. However, it is now apparent that genetic variability alone does not account for the whole variation in responses to targeted anti-cancer drugs [8, 9]. Non-genetic heterogeneity has two broad sources, epigenetic and stochastic, the latter being due to intrinsic factors such as noise in gene expression [10–13] and asymmetric cell division [14, 15]. These sources of heterogeneity can produce phenotype diversity even in genetically identical cells [8, 9, 16]. Not surprisingly, the analysis of the consequences of non-genetic cell-to-cell variability in the cellular response to drugs and its potential impact for the treatment of human diseases including cancer has become a crucial issue to understanding drug resistance phenomena and developing new targeted agents [1, 3, 17].

Beyond its well-documented role in development [18–20], bivalent chromatin is an emerging epigenetic trait of cancer that has been identified as a druggable therapeutic target [19, 21]. Genomic studies have found that there exists significant overlap between bivalent domains in pluripotent stem cells and regions in cancer exhibiting abnormal patterns of methylation, which pinpoints bivalency as a promising marker of tumourigenesis. Furthermore, different bivalent chromatin regulators have been identified as targets for cancer therapeutics [22–24]. An outstanding example of such regulator is EZH2 (a histone methyl transferase which is the catalytically active component of the PRC2 complex), which has been found to be mutated or overexpressed in a number of cancers [23]. Specifically, somatic EZH2 mutations have a major role in promoting lymphoid transformation in germinal-center leukemias [21]. Another family of epigenetic regulators that has emerged as a potential target are the so-called lysine demethylases (KDMs), whose expression has been found to be dysregulated in several types of neoplasms [22, 24]. Flavahan et al. [25] have recently proposed bivalent chromatin regulators as key factors in epigenetic plasticity, i.e. the epigenetically-driven alteration of the stability of cellular states (phenotypes). Variations in the activity of certain epigenetic enzymes such as EZH2 can lead to *repressive* states, where the epigenetic barriers are raised resulting in cells locked in a certain state, regardless of the presence of signalling cues instructing them to exit

such states. By contrast, such alterations can also produce *permissive* states in which the epigenetic barriers are lowered so that cellular states change by the mere presence of random noise. The latter states often lead to pathological plasticity and cell reprogramming [25–27].

The so-called Waddington or epigenetic landscape, a conceptual framework allowing the integration of both genetic and non-genetic variability, was proposed over seven decades ago [28]. In analogy to the potential energy landscape of physical systems, Waddington put forward a representation of a cellular state in the form of an *effective potential landscape* where the local minima correspond to cellular phenotypes. Phenotypic switch transitions occur when cells transit to other minima by jumping over the barriers separating adjacent basins. Such transitions are driven by intrinsic or extrinsic fluctuations [29, 30]. Noteworthy, the topography of such landscapes depends on a complex set of biochemical interactions and, in particular, on the values of the corresponding set of rate constants [17, 31–34]. These constants strongly depend on protein structure (e.g. the accessibility of a binding domain), which is encoded within the DNA [32]. Thus, an epigenetic landscape emerges from a particular genotype [17], and therefore can be interpreted as a representation of the genotype-phenotype map [35–40]. Beyond their dependence on DNA sequence, in the case of biochemical reactions involving enzymatic catalysis, the associated rate constants depend also on the concentration of metabolic cofactors [33, 34], which may differ among cells thus adding a further source of cell-to-cell heterogeneity.

In order to shed some light on the role of bivalent chromatin as a therapeutic target, we propose a mathematical model of a simple gene regulatory circuit with a bivalent promoter (see Fig 1a and 1b). Specifically, our model addresses mutual nonlinear feedbacks between marked nucleosomes and transcription factors (TFs), which drive not only the rates of both addition of new marks and TF synthesis [41–45], but also the heterogeneity of cellular populations [17, 33, 34, 46, 47].

The determination of epigenetic regulatory mechanisms has triggered an interest in developing mathematical models regarding both epigenetic regulation (ER) of gene expression [27, 33, 34, 41–43, 45, 48, 49, 52, 53] and epigenetic memory [48, 49, 52, 54–58]. Specifically, Sneppen et al. [41] were the first to propose a computational model to address the coupling between transcription factor and epigenetic regulation and how it produces ultrasensitive behaviour, but they did not consider bivalent chromatin. Such a coupling has been further studied in the context of bivalent chromatin [42, 43, 45]. Although these works, similarly to the model presented here, describe bistability in gene regulatory systems with TF self-regulation, it should be noted that they consider a self-activating TF with high intrinsic cooperativity (Hill coefficient $n = 3$) [42, 43]. Moreover, noise-induced phenomena in gene regulatory networks have been extensively studied [12, 59–63]. In particular, Biancalani and Assaf [12] have studied noise-induced bistability in a regulatory network (toggle switch) of monomeric, self-activating, mutually-inhibiting genes, but they did not consider ER.

Our model (whose main features are summarised in Fig 1) proves that bivalent chromatin regulation can induce complex behaviour even in the simplest circuits of gene regulation, which would not exhibit such features in the absence of bivalent regulation. We consider a model of a self-regulatory, monomeric TF with a bivalent promoter (see Fig 1a), characterised by a number of both positive and negative feedbacks identified in [42, 43] (and schematically illustrated in Fig 1b). The resulting model, in spite its apparent simplicity, exhibits considerable complexity regarding its nonlinearities and multiplicity of time scales. In order to make analytical progress, we exploit the latter and, by means of an asymptotic model reduction and singular perturbation analysis, we reduce the model to a one variable stochastic system (Fig 1c). By doing so, we have been able to determine, both numerically and analytically, that the

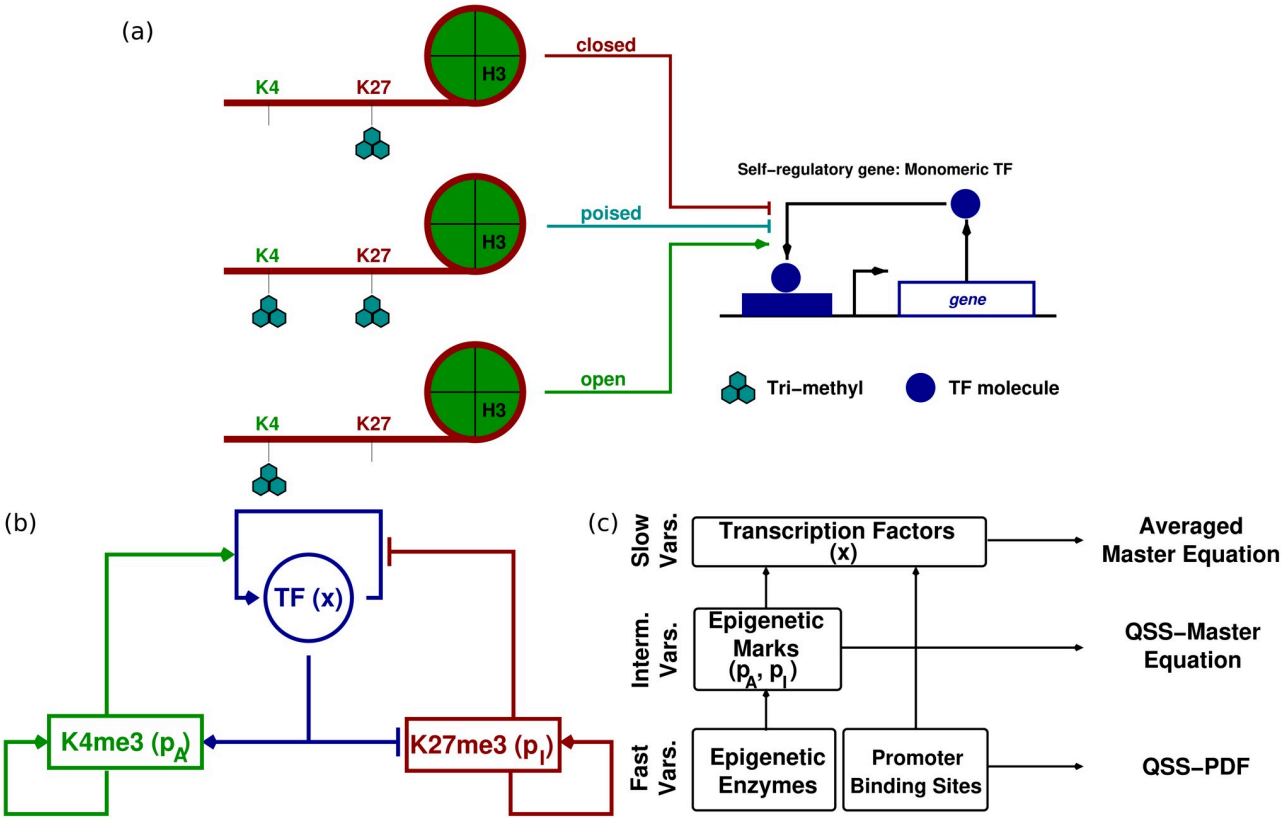

Fig 1. Summary of the model formulation. Panel (a) shows a schematic representation of the epigenetic-regulatory modifications considered in our model (i.e. trimethylation of H3K4 and H3K27), which affect promoter/enhancer regions. We focus on a transcription factor (TF) which is self-regulatory and monomeric. This panel also shows the different states of bivalent chromatin (*open* (*closed*) if H3K4me3 (H3K27me3) predominates, *poised* if both marks are present) and how they affect TF expression. Diagram (b) depicts a scheme showing the feedbacks between ER modifications and TF (full details given in Section S.1.1 in S1 Text). Plot (c) displays a schematic representation of the model reduction approximation, based on the presence of multiple time scales. Such a separation of time scales allows for a hierarchical elimination of the faster variables (full details given in Section S.1.2 in S1 Text). Here "QSS" stands for *quasi-steady state*; and "PDF" for *probability density function*.

https://doi.org/10.1371/journal.pcbi.1008408.g001

system exhibits three different behaviours: monostability, bistability, and noise-induced bistability [64] (Fig 2a). Specifically, we show that the activity of the epigenetic enzymes directly controls the effective cooperativity of the gene regulatory circuit, which impinges on its ability to produce bistable behaviour (Fig 2b).

Our analysis of a bivalent TF is based on the explicit calculation of the Waddington landscape for the system under consideration, which allows us to exhaustively classify the set of possible landscape topographies. We account for the effects of heterogeneous behaviour in the epigenetic-regulatory system [46, 47] by means of an ensemble approach previously developed [33, 34], in which we take advantage of the direct connection between landscape topography and the rate constants that characterise the underlying biochemical networks from which it emerges. After validating our ensemble approach against quantitative experimental data from Refs. [20, 21, 65], we finally address the issue of what epigenetic strategies are more effective regarding their ability to overcome heterogeneity. We conclude that those involving tackling the activity of demethylases are more efficient than those that targeting the activity of methyltransferases.

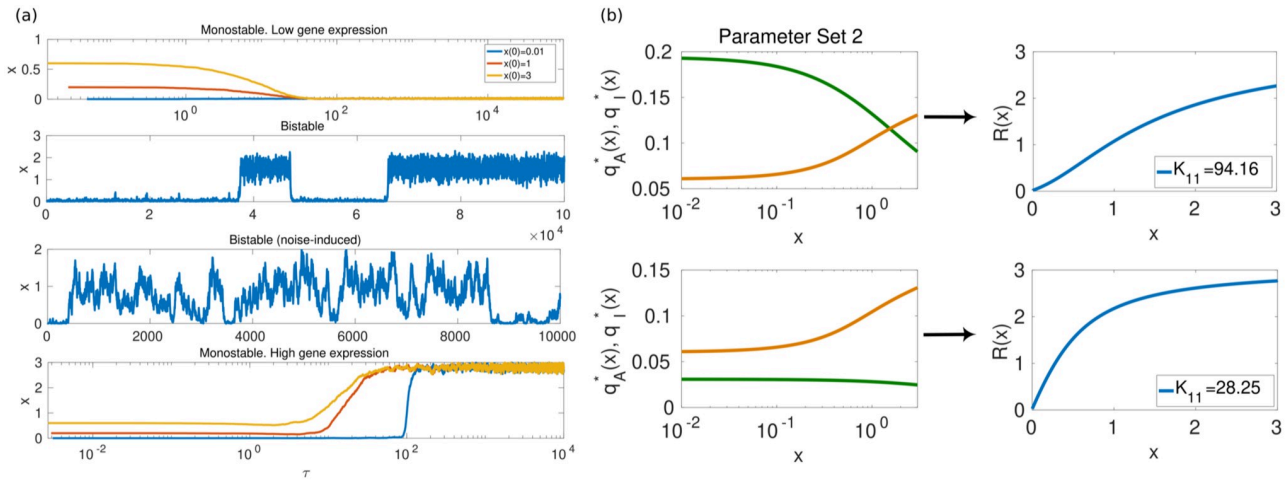

Fig 2. Summary of the model results. Plots in (a) show results of direct simulation of the process (carried out by means of the Gillespie algorithm [50, 51]). These simulations illustrate the four type of behaviours afforded by the stochastic model (from top to bottom): inactive TF, bistability, noise-induced bistability, and active TF. Plots in (b) illustrate one of our main results, namely, that the TF exhibits emergent, non-linear behaviour (e.g. bistability) which could not be observed in the absence of bivalent chromatin. Specifically, we show that such behaviour is associated to the tunability of the effective cooperativity, n_{eff}, of the TF regulatory circuit: by altering the activity of the chromatin-modifying enzymes we can control the quantity n_{eff}. In the particular case shown in the figure, by varying K_{11} (which corresponds to the K_M of the KDM that removes H3K27me3), the effective cooperativity changes from $n_{eff} > 1$ (upper plot) to $n_{eff} \leq 1$ (lower plot). The response curve, $R(x)$, and the n_{eff} of the TF are defined by $R(x) = \rho\left(1 + C_1 \frac{q_A^*(x)x}{\lambda_x q_I^*(x) + q_A^*(x)x}\right) = \rho\left(1 + C_{eff} \frac{x^{n_{eff}}}{\lambda_{eff} + x^{n_{eff}}}\right)$. Here $q_A^*(x)$ and $q_I^*(x)$ are shown in green and orange lines, respectively.

https://doi.org/10.1371/journal.pcbi.1008408.g002

Materials and methods

Model formulation

Here, we focus on an epigenetic regulation (ER) model that consists of four enzymatic reactions, which account for the addition and removal of a 3-methyl, to be referred as "me3", epigenetic mark to two specific lysine residues in the tail of the H3 histone (H3K4 and H3K27, see Fig 1a). Each of these enzymatic reactions is modelled by means of the well-known Michaelis-Menten (MM) model of enzymatic catalysis (see [66] and S1 Text for details specific to our model). We apply this model to address how specific enzymes catalyse the addition of the me3 mark to each residue (MLL2 to H3K4 and EZH2 to H3K27 [25]), and the removal of me3 from modified residues (specifically, KDM2/KMD5 from H3K4me3 and KDM6 from H3K27me3 [67, 68]). Beyond the regular mechanisms of enzyme kinetics, epigenetic regulation exhibits several feedback mechanisms that need to be taken into account [41, 54]. Modified residues enhance recruitment of epigenetic enzymes, providing a positive feedback mechanism where residue modification increases the rate of further me3 addition (see Fig 1b). Following previous models of ER [33, 34], we account for such positive feedbacks by taking the rate constants associated to each of the me3-addition MM reactions to change linearly with the number of corresponding modified residues (see Table A in S1 Text). Furthermore, recruitment of epigenetic enzymes to H3K4 is also enhanced by the presence of transcription factors [41–43] (see Fig 1b). Such positive feedback is also accounted for by assuming the rate constants of the MM reaction associated with H3K4→H3K4me3 to change linearly with the number of TF molecules. By contrast, TF presence hinders recruitment of me3-addition to H3K27 [42, 43] (see Fig 1b). To take into account this negative feedback, we have assumed that the rate corresponding to the back reaction of the MM reaction associated to H3K27→H3K27me3 depends linearly on the number of TF molecules (see Table A in S1 Text).

Regarding the gene regulatory system, we consider a simple self-regulatory gene (see Fig 1a), i.e. a gene such that its protein stimulates its own expression, modelled by a simple Hill model (with Hill constant $\alpha = 1$, since we are considering a monomeric TF) [69] with natural decay and basal production of the TF molecules. As shown in Fig 1, the feedback between TF dynamics and ER is accounted for by assuming that the rate of TF binding to the gene's promoter region is proportional to the number of H3K4me3, whilst the rate TF unbinding is proportional to the number of H3K27me3. A fully detailed account of the model formulation is provided in Section S.1 in S1 Text.

Asymptotic analysis and model reduction

The model resulting from the previous discussion is rather complicated. In order to make analytical progress, we exploit the presence of separation of time scales. In particular, we resort to asymptotic model reduction techniques and singular perturbation analysis (see Fig 1c for a schematic representation). A fully detailed derivation is presented in Section S.1.1 in S1 Text, which we summarise here. Under the assumptions considered in detail in S1 Text, we have:

1. A *fast dynamics* in which the histone-modifying enzymes and associated complexes reach quasi-equilibrium with the substrates, products, TF, and marks. Also, the binding sites in the promoter of the gene reach quasi-equilibrium with TFs and ER products.
2. An *intermediate dynamics* in which epigenetic substrates and products reach quasi-equilibrium with TF and marks.
3. A *slow dynamics* in which the TF evolves in quasi-equilibrium with the fast and intermediate variables.

We proceed with our analysis in three stages. In the first step, the *fast dynamics* is studied under adiabatic conditions with respect to the *intermediate* and *slow* variables, i.e. the latter variables are considered as frozen and the fast variables can be analysed, specifically regarding their quasi-steady state distribution (QSSD), with the intermediate and slow variables set to constant. In the second stage, the intermediate variables are studied under adiabatic conditions with respect to the slow variables and by sampling the fast variables from their fast QSSD. We consider the usual assumptions regarding separation of time scales and the associated quasi-steady state (QSS) approximations normally involved in the analysis of MM and Hill systems (see [66, 69]). The third stage consists of studying the slow variables with the fast and intermediate ones in quasi-equilibrium, i.e. sampled from their associated QSSD.

Reduced model: Mean-field limit

We can reduce the dynamics of the whole system to that of three variables: the number of TF molecules, corresponding to the slow variable x, and the number of H3K4me3 and H3K27me3 residues, corresponding to the intermediate variables p_A and p_I (all other intermediate variables can be ignored thanks to conservation laws). All variables are defined in Section S.1.1 in S1 Text. The mean-field limit is obtained from letting the characteristic scales for the number of H3K4/H3K27 and TF molecules tend to infinity (see Section S.1.2.1 in S1 Text for a detailed derivation). In this limit, we keep the notation x for the TF and denote as q_A and q_I the limit of the intermediate variables. The model reduction procedure leads to the following system of

three differential equations (see Eqs. (S.24)-(S.26) in S1 Text):

$$\frac{dx}{d\tau} = B_x(x, q_A, q_I) - D_x(x, q_A, q_I), \tag{1}$$

$$\epsilon_2 \frac{dq_A}{d\tau} = B_A(x, q_A) - D_A(x, q_A), \tag{2}$$

$$\epsilon_2 \frac{dq_I}{d\tau} = B_I(x, q_I) - D_I(x, q_I), \tag{3}$$

where

$$B_x = \rho\left[1 + (C_1 + C_4 q_I)\frac{q_A x}{\lambda_x q_I + q_A x}\right],$$

$$B_A = \Lambda_A \frac{(\rho_A - q_A)(A_1 + q_A x)(A_3 + q_A x)}{(\rho_A - q_A)(A_1 + q_A x) + B_2 + K_2 q_A x},$$

and

$$B_I = \Lambda_I \frac{(\rho_I - q_I)(A_7 + q_I)(A_9 + q_I)}{(\rho_I - q_I)(A_7 + q_I) + B_8 + (K_8 x + K_9) q_I}.$$

Also,

$$D_x = \rho\left[C_2 x + C_4 q_I \frac{q_A x}{\lambda_x q_I + q_A x}\right], D_A = \Lambda_A \lambda_A \frac{K_6 q_A}{q_A + K_5}, \text{ and } D_I = \Lambda_I \lambda_I \frac{K_{12} q_I}{q_I + K_{11}}.$$

The QSS concentration of H3K4me3, $q_A^*(x)$; and of H3K27me3, $q_I^*(x)$, are the solutions of $\frac{dq_A}{d\tau} = 0$ and $\frac{dq_I}{d\tau} = 0$, respectively. Note that, stemming from the assumption that $\epsilon_2 = \frac{\Omega_S}{\Omega_T} \ll 1$, where Ω_S and Ω_T are characteristic scales for the number of H3K4 and H3K27, and TF molecules, respectively, the resulting reduced system, given by Eqs (1)–(3), still exhibits slow-fast features (see Section S.1 in S1 Text).

Reduced stochastic model

The effects of intrinsic fluctuations on the mean-field limit can be studied by means of the reduced stochastic model (see sections S.1.1 and S.1.2.1 in S1 Text for a detailed derivation and Section S.1.2.2 in S1 Text for the details of the singular perturbation analysis). The reduced stochastic model alse exhibits slow-fast features. The corresponding Master Equation (ME) reads:

$$\frac{\partial \Phi}{\partial \tau} = \mathcal{H}_x(x, \partial_x)\Phi + \frac{1}{\epsilon_2}\left(\mathcal{H}_A(p_A, \partial_{p_A}) + \mathcal{H}_I(p_I, \partial_{p_I})\right)\Phi \tag{4}$$

where the operators $\mathcal{H}_x$, $\mathcal{H}_A$, and $\mathcal{H}_I$ are given by

$$\mathcal{H}_x\Phi = \Omega_T(\mathcal{E}_{x_+} B_x(x, p_A, p_I)\Phi(x, p_A, p_I, \tau) + \mathcal{E}_{x_-} D_x(x, p_A, p_I)\Phi(x, p_A, p_I, \tau)),$$

$$\mathcal{H}_A\Phi = \Omega_S(\mathcal{E}_{A_+} B_A(x, p_A)\Phi(x, p_A, p_I, \tau) + \mathcal{E}_{A_-} D_A(x, p_A)\Phi(x, p_A, p_I, \tau)),$$

and

$$\mathcal{H}_I\Phi = \Omega_S(\mathcal{E}_{I_+}B_I(x,p_I)\Phi(x,p_A,p_I,\tau) + \mathcal{E}_{I_-}D_I(x,p_I)\Phi(x,p_A,p_I,\tau)).$$

The step operators are defined in the usual manner [70, 71]: $\mathcal{E}_{x_\pm} = e^{\pm\partial_x} - 1$, $\mathcal{E}_{A_\pm} = e^{\pm\partial_{p_A}} - 1$, and $\mathcal{E}_{I_\pm} = e^{\pm\partial_{p_I}} - 1$ (the exponential operator is defined in Section S.1.2.2 in the S1 Text).

In order to proceed forward we expand the PDF $\Phi(x, p_A, p_I, \tau)$ in powers of ϵ_2: $\Phi = \Phi_0 + \epsilon_2\Phi_1 + \mathcal{O}(\epsilon_2^2)$ [64, 72]. In Section S.1.2.2 in S1 Text, we show that, at the lowest order, Φ_0 can be written as $\Phi_0(x,p_A,p_I,\tau) = \phi_x(x,\tau)\phi_A(p_A|x)\phi_I(p_I|x)$, with ϕ_A and ϕ_I such that $\mathcal{H}_A\phi_A = 0$ and $\mathcal{H}_I\phi_I = 0$. The WKB solution to the latter equations is given by

$$\phi_J = \frac{\mathcal{N}_J \exp\left(-\Omega_S \int_0^{p_J} \log\left(\frac{D_J(s,x)}{B_J(s,x)}\right) ds\right)}{\sqrt{B_J(p_J,x)D_J(p_J,x)}}$$

with $J = A, I$. However, as usual with singularly-perturbed problems such as Eq (4), the lowest order approximation does not provide any information regarding $\phi_x(x,\tau)$ and we need to resort to the next order [72, 73]. At steady state (see Section 1.2.2 in S1 Text), by considering the appropriate solvability conditions, we can show that, to the lowest order,

$$\phi_x(x) = \mathcal{N}_x e^{-\Omega_T \mathcal{U}(x,\Omega_T)}, \tag{5}$$

where the effective potential, $\mathcal{U}$, is given by:

$$\mathcal{U} = -\mathcal{S} + \frac{\log\langle B_x\rangle + \log\langle D_x\rangle}{2\Omega_T},\ \mathcal{S} = \int_0^x \log\frac{\langle B_x\rangle}{\langle D_x\rangle} ds, \tag{6}$$

where $\langle B_x\rangle = \int_{\mathcal{D}} B_x\phi_A\phi_I dp_A dp_I = \rho\left[1 + (C_1 + C_4 q_I^*(x))\frac{q_A^*(x)x}{\lambda_x q_I*(x) + q_A^*(x)x}\right]$ and

$$\langle D_x\rangle = \int_{\mathcal{D}} D_x\phi_A\phi_I dp_A dp_I = \rho\left[C_2 x + C_4 q_I^*(x)\frac{q_A^*(x)x}{\lambda_x q_I^*(x) + q_A^*(x)x}\right].$$

A fully detailed derivation of the asymptotic calculation is given in S1 Text, Section S.1.2.

The ensemble approach: Modelling heterogeneity and parameter sensitivity analysis

Our ensemble approach serves two distinct but not unrelated purposes, namely, to perform a parameter sensitivity analysis and to model heterogeneity observed in epigenetic regulatory systems [46, 47]. Regarding the former, given the complexity of our model, we need to consider carefully robustness to variations in parameter values. We consider such issue using an ensemble approach introduced in [33, 34]. Briefly, we generate an ensemble of parameter sets. A parameter set is described by means of a vector, θ, defined as (see Table B in S1 Text):

$$\theta = (A_1, A_3, B_2, K_2, K_5, K_6, \lambda_A, \lambda_x, A_7, A_9, B_8, K_8, K_9, K_{11}, K_{12}, \lambda_I).$$

Each component of θ is independently generated by sampling from a uniform prior distribution within a certain prescribed range. Randomly generated parameter sets are accepted only if the q_A and q_I are monostable (see Section S.1.4 in S1 Text). The sets of parameter values thus generated are then classified into several sub-ensembles depending on the number of roots of $\partial_x\mathcal{U} = 0$, i.e. the number of modes of ϕ_x, and $\partial_x\mathcal{S} = 0$, i.e. the number of mean-field steady-states. We consider a monostable sub-ensemble composed by those θs such that both

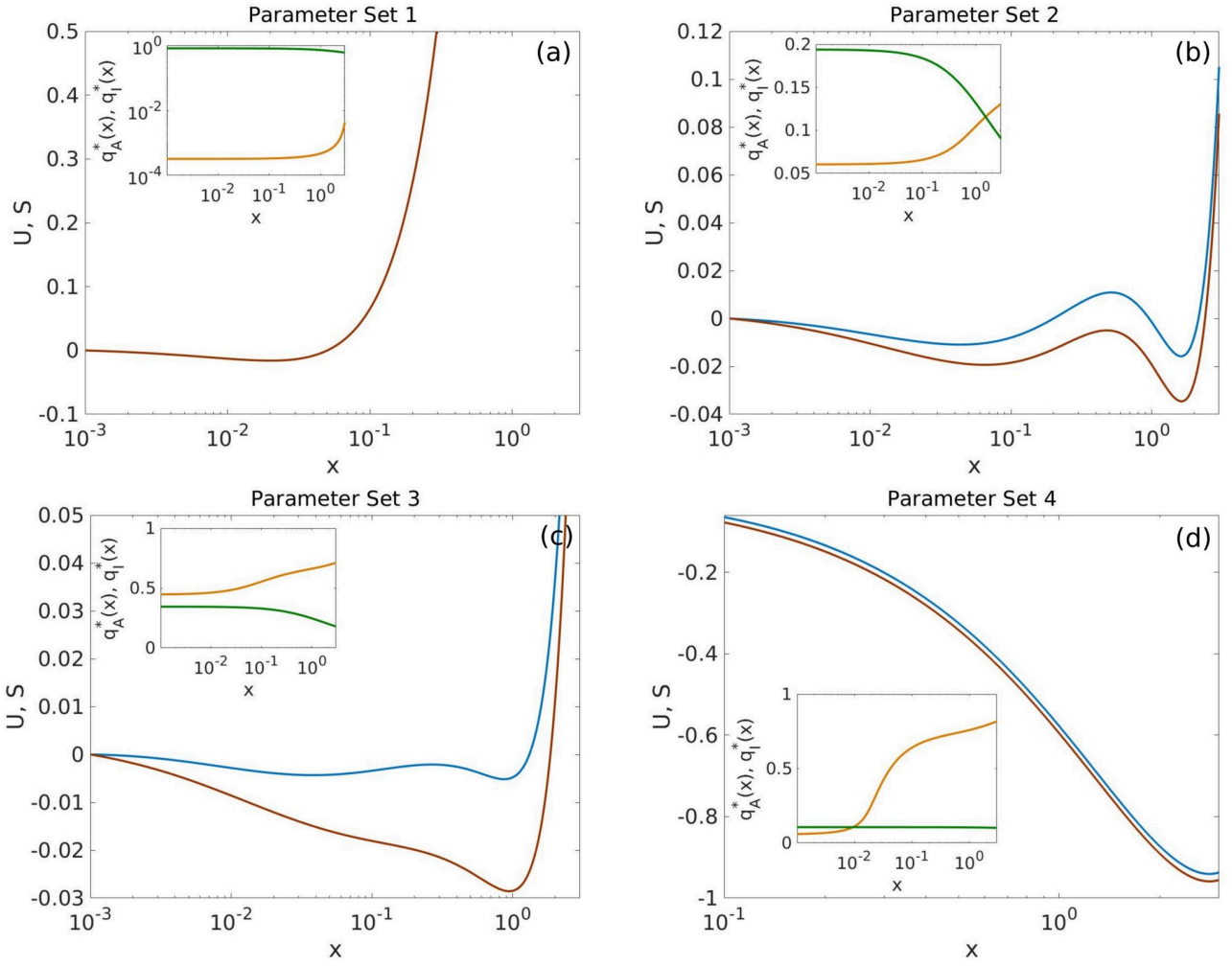

Fig 3. Representative examples of the four sub-ensembles. Plot (a) shows an example of a monostable, low gene expression system, belonging to the Low GE sub-ensemble. Plots (b) and (c) show examples of systems within the bistable and the noise-induced Bistable sub-ensembles, respectively. Plot (d) shows an example of a monostable, high gene expression system, belonging to the high GE sub-ensemble. See main text for details. Colour code: Red lines show $\mathcal{S}'(x)$, blue lines correspond to $\mathcal{U}'$. Green and orange lines within the insets represent $q_I^*(x)$ and $q_A^*(x)$, respectively. Parameter values are given in Tables F-I of S1 Text.

https://doi.org/10.1371/journal.pcbi.1008408.g003

$\partial_x \mathcal{U} = 0$ and $\partial_x \mathcal{S} = 0$ have only one real, positive root. We split this set of parameters further by considering a high gene expression (high GE) sub-ensemble if the modal point $x_* \geq x_{THR}$; and a low gene expression (low GE) sub-ensemble $x_* < x_{THR}$. We consider a Bistable sub-ensemble composed by those θs such that both equations have three roots. Last, the noise-induced Bistable sub-ensemble comprises θs such that $\partial_x \mathcal{U} = 0$ has three roots while $\partial_x \mathcal{S} = 0$ has only one root. Representative examples of landscapes associated with systems, i.e. θ, belonging to each of four sub-ensembles are shown in Fig 3. We then analyse the ensembles in terms of the comparison of the marginal posterior PDFs for each of the components of θ and also their correlations. We expect that by discerning which parameters present statistically significant differences between sub-ensembles, we can identify which of them are key to produce the behaviour associated to a particular sub-ensemble [33, 34]. We refer the reader to S1 Text, Section S.1.4.2, for a full account of the details of the classification procedure and further statistical analysis.

In order to characterise phenotypic heterogeneity in a biologically meaningful way, we use a proxy or estimate for the enzymatic activity of the four chromatin modifiers included in our model. Specifically, we take that our estimate of the rate of activity of the epigenetic enzymes is the maximum of the average of the quantities B_A, B_I, D_A, and D_I defined above (see Eqs (2) and (3)). These four quantities correspond to the rates at which me3 marks are added and removed from the lysine residues and, therefore, they are direct measures of the rates of activity of the chromatin-modifying enzymes. Our proxy of the enzyme activity involves then averaging B_A, B_I, D_A, and D_I with respect to the distribution ϕ_x (see Eq (6) and then taking the maximum over q. The mathematical definitions of these estimates are given in S1 Table.

Experimental evidence of heterogeneity in ER systems comes from a number of sources. It has been directly observed in single-cell CHIP-seq experiments [47]. Other studies have provided evidence that the *de novo* reprogramming potential is higher within selected subpopulations of cells and that such pre-existing epigenetic heterogeneity can be tuned to make cells more responsive to reprogramming stimuli [46]. Furthermore, Beguelin et al. [21] have reported that the efficiency of drugs that target chromatin regulators, specifically EZH2 inhibitors, is very heterogeneous: their IC_{50} varies from one cell type to another in two orders of magnitude (see figure S.1 in the supplementary information of Ref. [21]). In order to mimic, at least in part, the existing ER heterogeneity within a cell population from a particular tissue, the generated ensemble of ER systems can be used to identify properties at the population level. Our approach follows closely that of Ref. [33]. The above procedure provides us with an ensemble of parameter sets, θ, that are compatible with each of the four behaviours we have found (Low GE, High GE, bistability, and noise-induced bistability). In order to check whether the heterogeneity within the ensemble is compatible with existing biological variability, we compare with quantitative experimental data provided by Beguelin et al. [21].

Results

Validation of the ensemble model

We first validate our approach against qualitative and quantitative results [20, 21, 25, 65, 74]. Fig 4a–4c show summary statistics of the monostable and Bistable sub-ensembles. Specifically, Fig 4a shows the distribution of modes of $\phi_x(x)$, x_*, within the monostable sub-ensemble. Note that this distribution is a distribution of x_* as the parameters θ are varied so it is bimodal with respect to the sub-ensemble. As we can see this distribution is bimodal, which supports the definition of two monostable sub-ensembles: the low gene expression (Low GE) sub-ensemble and the high gene expression (High GE) one.

Fig 4b shows a scatter plot of the effective potential barriers, $\Delta\mathcal{U}_0$ and $\Delta\mathcal{U}_1$, within the Bistable sub-ensemble. According to [25], there are several pathological situations that can be described on the basis of such quantities. Repressive states, associated with higher barriers, and permissive states, corresponding to lower barriers, appear in response to dysregulation of chromatin modifiers. Both states are represented in our ensemble by those ER systems which lay at the tails of Fig 4b (or within the tails of the histogram shown in Fig 4c). Other anomalies of the epigenetic landscape involve lowering of both barriers which facilitate noise-driven exploration of different phenotypes. These systems are also represented in our bistable ensemble by those systems located in the lower left corner of Fig 4b, i.e. such that $\Delta\mathcal{U}_0$ and $\Delta\mathcal{U}_1$ are both small and of the same order of magnitude.

Beyond qualitative arguments, quantitative validation is possible. Consider the data from Bernstein et al. [20] regarding the number and relative expression levels of genes with bivalent marks, H3K4me3-dominated genes, H3K27me3-dominated genes, and unmarked genes (methylation status). Such data was provided for both embryonic stem cells (ESCs) and several

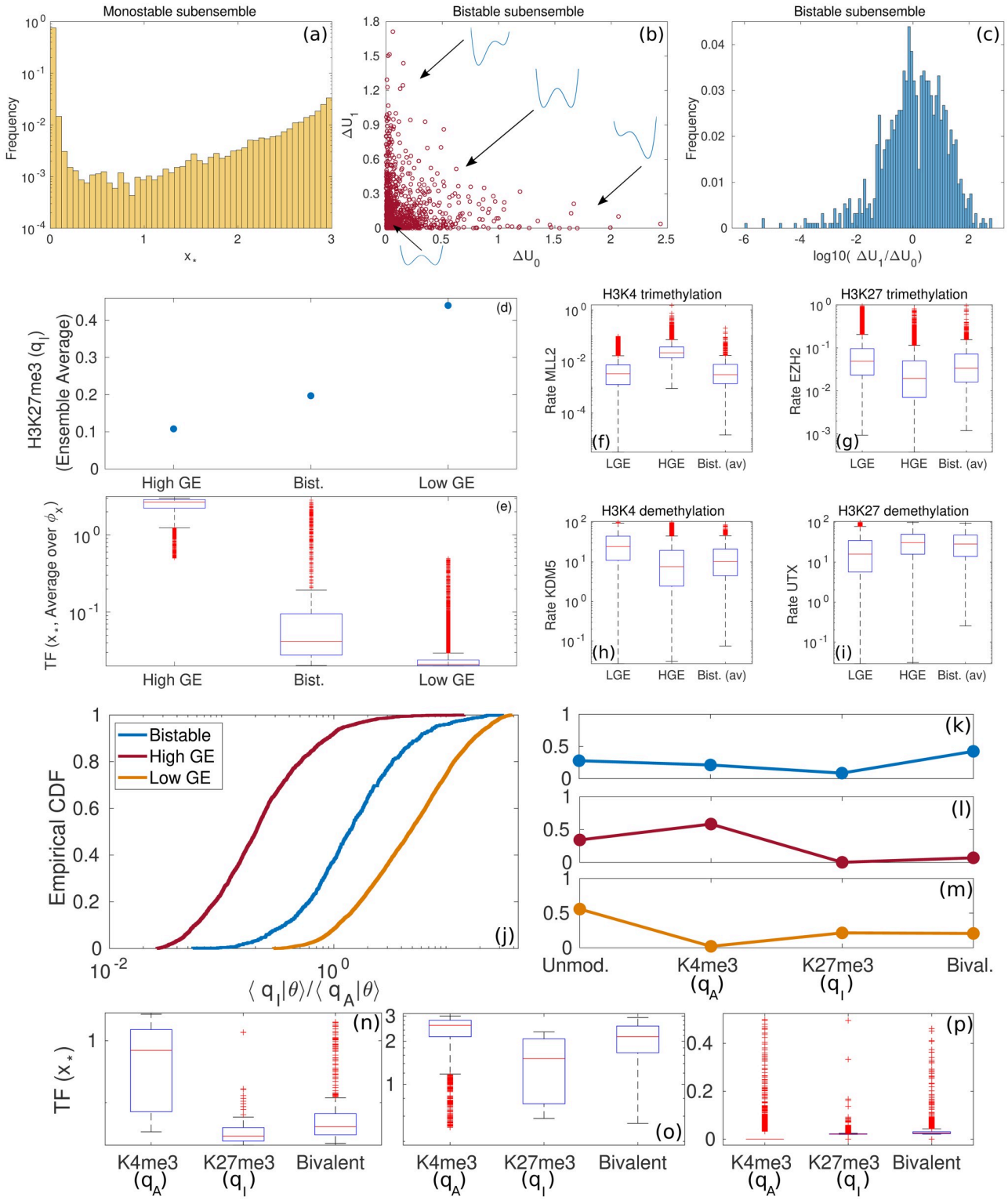

Fig 4. Validation of the ensemble model. Plots (a), (b), and (c) show summary statistics regarding the monostable and Bistable sub-ensembles. Plot (a) shows the distribution of modes, x_*, within the monostable sub-ensemble. Plot (b) shows the scatter plot of the effective potential barriers, $\Delta\mathcal{U}_0$ and $\Delta\mathcal{U}_1$, within the Bistable sub-ensemble. Plot (c) shows the histogram of the ratio $\Delta\mathcal{U}_1/\Delta\mathcal{U}_0$ within the Bistable sub-ensemble. Panels (d) and (e) show data regarding statistics of the Bistable, High GE, and Low GE sub-ensembles. Plot (d) displays sub-ensemble averages of the H3K27me3 marks and (e) shows the boxplots of the TF levels (specifically, we use the modal TF concentration, x_* as a proxy) for each of the sub-ensembles. These data are to be compared with the experimental results from [21]. Plots (f)-(i) show the boxplots of the distributions of activity of the chromatin modifiers for each of

the sub-ensembles (see S1 Table). Finally, plots (j) to (p) report statistics of the Bistable, High GE, and Low GE sub-ensembles regarding their comparison to quantitative data provided in [20]. Plot (j) shows the empirical cumulative density function (CDF) for the ratio $\langle q_I|\theta\rangle_x/\langle q_A|\theta\rangle_x$ for each of the sub-ensembles. Plots (k), (l), and (m) show the proportion of elements of each sub-ensemble with no detectable methylation marks (which we define as those systems such that $\langle q_A|\theta\rangle_x < 0.05$), dominant K4me3 marks ($\langle q_I|\theta\rangle_x < 0.8$), dominant H3K27me3 marks ($\langle q_I|\theta\rangle_x/\langle q_A|\theta\rangle_x < 5$), and bivalent marks. These are to be compared with data from figure 2 in [20]. Plots (n), (o), and (p) show the modal TF expression, x_*, for H3K4me3 marked systems, H3K27me3 marked systems, and bivalent systems for the bistable, High GE, and Low GE sub-ensembles, respectively. These results are to be compared with figure 4 in [20]. We have used the abbrevations "LGE" and "HGE" for Low GE and High GE, respectively.

https://doi.org/10.1371/journal.pcbi.1008408.g004

types of differentiated cells (DCs) (shown in figures 2 and 4 in [20], respectively). Fig 4j–4m address our results regarding methylation status patterns. Fig 4k–4m show results of the frequency of each methylation status for all three sub-ensembles. The pattern exhibited by the Bistable sub-ensemble is the same as the ESCs data from Ref. [20] (see figure 2 in Ref. [20]): the frequency of unmarked, bivalent and H3K4me3-dominated is of the same order, whilst the frequency of negatively (H3K27me3) marked systems is much lower. High GE sub-ensemble shows the same pattern as DCs: the frequency of positive marks is much increased with respect to ESCs, whereas the frequency of bivalent marks is considerably reduced to the same level as the frequency of negative marks. By contrast, the Low GE pattern is not compatible with any of the patterns reported by Bernstein *et al.* [20].

Fig 4n–4p address the comparison with the levels of TF expression. We use the distribution of modal TF expression, x_*, for each methylation status. Fig 4n shows that the patterns of the Bistable sub-ensemble match the experimental behaviour of ESCs (see figure 4 in Ref. [20]), as the expression of H3K4me3-marked TFs is between 1 and 2 orders of magnitude larger than the levels exhibited by bivalent and H3K27me3-marked TFs. We also observe that TF expression is largely suppressed in bivalent systems, their levels being only slightly larger than that of H3K27me3-marked TFs. The pattern of TF expression within the High GE expression shown in Fig 4o fits that of DCs: H3K4me3-marked systems exhibit higher TF expression than that of H3K27me3-marked and bivalent systems, but the overall levels of expression are much more uniform than in the case of the Bistable sub-ensemble. The pattern of TF expression of the Low GE ensemble shown in Fig 4p are not consistent with any of the results of Bernstein *et al.*

Further validation of the ensemble model can be obtained by comparing to Beguelin et al. [21], who studied the role of somatic mutations of EZH2 on lymphoid transformation in germinal centre leukemias. They determined that EZH2 mutants, specifically Y641F and Y641N, lock B cells in an undifferentiated state during the germinal centre reaction. Such undifferentiated state can eventually lead to unchecked cell duplication (by silencing the cell-cycle inhibitor p27) and malignant progression. Beguelin *et al.* quantified the levels of H3K27me3 in cells carrying the wild-type (WT) EZH2 and cells carrying the mutants Y641F and Y641N (Figure 3b in [21]). They also collected quantitative information of the relative levels of expression of certain differentiation TFs (specifically IRF4, figure S.4 in the supplementary information of Ref. [21]). These data can be compared with our ensemble model, as shown in Fig 4d and 4e.

Fig 4d shows the sub-ensemble average of the number of H3K27me3-marked residues (see S1 Text, Section S.1.5 for details) for the Bistable, High GE, and Low GE sub-ensembles. The predicted levels of H3K27me3 in the Bistable sub-ensemble doubles those in the High GE. This is consistent with the relative increase of H3K27me3 in the Y641F and Y641N mutants relative to WT (although in absolute numbers, our model prediction is slightly lower than those measured experimentally, figure 3b in [21]). The Low GE sub-ensemble exhibits a 4-fold increase in H3K27me3 with respect to the High GE sub-ensemble, which is out of the scale observed experimentally. Fig 4e shows boxplots of TF expression (specifically, of the modal level of expression, x_*) for each sub-ensemble. Comparing the results for the High GE and

Bistable sub-ensembles, we notice that, consistently with Beguelin *et al.* (figure S.4 in the supplementary information of [21]), there are between 1 and 2 orders of magnitude of difference, average TF levels being higher in the High GE.

Finally, Fig 4f–4i show boxplots for activity of the chromatin modifiers (see Eqs (1)–(3) and S1 Table) for each of the four sub-ensembles. By inspection, whilst there are obvious differences between the Low GE PDFs and those corresponding to the High GE and the Bistable sub-ensembles, the difference between the latter ones is much less obvious. Specifically, activity of EZH2 is higher in the Bistable sub-ensemble than in its High GE counterpart. By contrast, MLL2 activity is lower in the Bistable sub-ensemble than in the High GE sub-ensemble. These results are consistent with the roles of EZH2 and MLL2 as poor prognosis factors in several types of cancers: while elevated activity of EZH2 is a poor prognosis indicator [75–79], impairing of MLL2 activity leads to poorer projected diagnosis [80–82].

Furthermore, quantitative analysis performed for four parameters related to the enzymatic kinetics of EZH2 (see Eq (3)) for each of the four sub-ensembles (see S1 Text, Section S.1.4 for full analysis) shows again no obvious differences between the Low GE PDFs and those corresponding to the High GE and the Bistable sub-ensembles. Statistical analysis (see S1 Text) shows significant differences, but with p-values very close to the significance level. This observation is consistent with direct *in vitro* measurements of the Michaelis-Menten constant, K_M, and the catalytic constant, k_{cat}, of the wild-type EZH2 and Y641F and Y641N mutants by [65], who found that in all variants of the enzyme, the K_Ms retained similar values within the error bars (see Fig F in S1 Text).

Taken together, these results validate two essential aspects of our model. First, the ensemble variability appears to be consistent with the amount of heterogeneity observed in the experiments carried out in [20, 21, 65]. Furthermore, these results allow us to identify the systems within the Bistable sub-ensemble (and probably also the Noise-Induced Bistable one) with ESCs/undifferentiated cells, whereas the High GE systems can be identified with differentiated cell types. The Low GE sub-ensemble exhibits properties which are incompatible with either type.

Bivalency allows for bistability and tunable cooperativity

Our analysis reveals that our model of a bivalent TF exhibits an array of complex behaviours, which are inaccessible to the gene regulatory system in the absence of bivalent ER (see [41]), and give rise to a variety of topographies of the epigenetic landscape, $\mathcal{U}_{eff}$. Such behaviours are illustrated in Figs 2a and 3. In particular, besides the expected monostable behaviour (with both low and high TF expression, Fig 3a and 3d, respectively), Fig 3b shows that the bivalent TF model exhibits bistability. Such behaviour is associated with effective cooperativity $n_{eff} > 1$ (see caption of Fig 2b), in contrast to the monomeric self-regulating gene with no bivalent ER (which has $n_{eff} = 1$). By means of a sensitivity analysis, we determine that variation of key parameters associated with the activity of ER enzymes, specifically, B_2, B_8, K_5 and K_{11} (see Eqs (2) and (3), provides us with ability to control n_{eff} thus allowing to suppress bistable behaviour, since variations of n_{eff} can drive the system through a saddle-node (s-n) bifurcation, thus removing pathological equilibria (see Fig 5). Such result is consistent with current experimental evidence, whereby controlling the activity of the ER enzymes, specifically of EZH2 [21, 83], has the effect of reducing pathologically-heightened epigenetic barriers and allow for physiological differentiation. Specifically, Fig 5 shows the change of the steady state concentration of TF as B_2 and B_8 vary. The s-n bifurcation causes sharp transitions at both the lower and upper yellow boundaries of Fig 5b, which enclose the region of bistability. The variety of dynamical behaviours exhibited by our system is depicted by several examples shown in the panels: (b1)

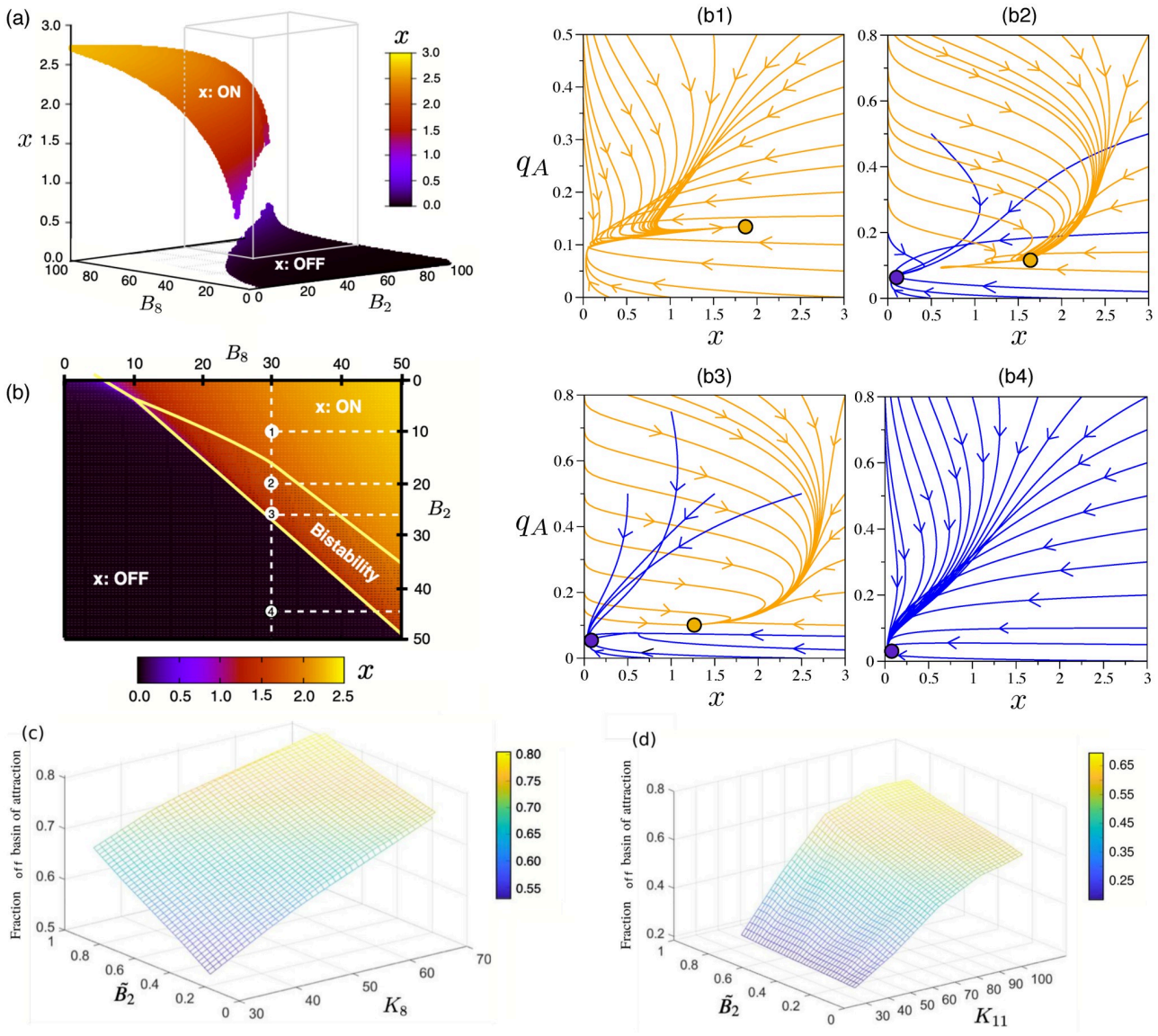

Fig 5. Equilibria in the parameter space (*B2*,*B8*). Panel (a) shows the equilibrium concentration of the TF (variable x) in the parameter space ($B2$,$B8$), the upper (resp., lower) sheet corresponding to the high (resp., low) level of expression, labelled as ON (resp., OFF) state. Panel (b) displays an enlarged view within the range contained in the cube in (a), namely $0 \leq B_2, B_8 \leq 50$. The region contained in the central orangish area corresponds to bistability. (b1-b4) Phase portraits showing the dynamics in the parameter space (x,q_A) for the combination of parameters B_2,B_8 indicated with dashed lines in (b), computed using $\epsilon = 0.1$. The orange and blue orbits correspond to the dynamics achieving the ON and OFF states, respectively. Note that both (b2) and (b3) fall into the region of bistability. Panels (c) and (d) show the relative size of the basin of attraction of the OFF equilibrium for parameter sets within the bistability region: (c) Parameter plane $B_8 - \tilde{B}_2$, where K_{11} is set to be 94.155549; (d) Parameter plane $K_{11} - \tilde{B}_2$, where B_8 is set to be 30. For the sake of visualisation, $\tilde{B}_2$ stands for a normalization of parameter B_2, see (S.34) in Section S.1.3 in the S1 Text Other constants are fixed according to the parameter set 2 (see Table I in S1 Text).

https://doi.org/10.1371/journal.pcbi.1008408.g005

monostability with TF at ON state (high level of expression); (b2)-(b3) with bistability behaviour; and (b4) monostability with the TF at OFF state (low level of expression).

In the case of bistable behaviour, it is interesting to analyse the variation of the basin of attraction (BA) of the high (ON) and low (OFF) TF concentration steady states as the activity of the chromatin-modifying enzymes changes. Specifically, for concreteness, we analyse how the BAs change as B_2 and B_8 vary (see Fig B in S1 Text), which impinge upon the activity of

MLL2 and EZH2, respectively. Within the bistability region, the probability of reaching either state is sensitive to parameter variation. In Fig 5c and 5d, we show the results of exploring the region of bistability within the parametric space (B_2,B_8,K_{11}) by computing the relative size, P_{off}, of the basin of attraction of the OFF state (note that $P_{off} + P_{on} = 1$) using a Monte Carlo procedure. This quantity provides an approximation of the probability that a given combination of TF molecules and methylated histones evolve towards the OFF state. From Fig 5, we show that, as we increase the value of any of the three factors (B_2, B_8 and K_{11}), the system is more likely to evolve towards an OFF state. This result illustrates that ON-OFF transitions can occur upon variation of the activity of epigenetic-regulatory enzymes in a deterministic way.

From the mechanistic point of view, a necessary (but not sufficient) condition for bistable behaviour ($n_{eff} \geq 1$) is that the QSS mark concentrations, $q_A^*(x)$ and $q_I^*(x)$ (see Eqs (2) and (3) and S1 Text), exhibit the X-like pattern we observe in Figs 2b and 3b. When this condition is satisfied, if x fluctuates below its crossover value, the system enters a regime that favours a continued decrease in gene expression since the negative marks dominate over the positive ones, and viceversa, thus inducing ultrasensitive behaviour associated with $n_{eff} \geq 1$ and bistability. From this perspective, the mechanism behind the role of the activity of the ER enzymes is clear: by changing the value of key parameters, we can alter such pattern and induce transitions in the system (s-n bifurcations) from bistable to monostable behaviour (Fig 3a and 3d).

Bivalency causes noise-induced bistability

Besides bistable behaviour, the bivalent TF model also exhibits noise-induced bistability, i.e. the ability of the system to sustain two stable steady-states only if the system is affected by noise. An example of this behaviour is shown in Fig 3c, where we show that $\phi_x(x)$ is bimodal for finite system size ($\Omega_T = 200$). Such behaviour is lost for vanishing levels of noise in the system (when $\Omega_T \to \infty$). This feature is confirmed by direct Gillespie simulations of the stochastic process described by Eq (4). Results are displayed in Figs 2a and 6, where we present simulations of the system for different system sizes, which show that, in agreement with our

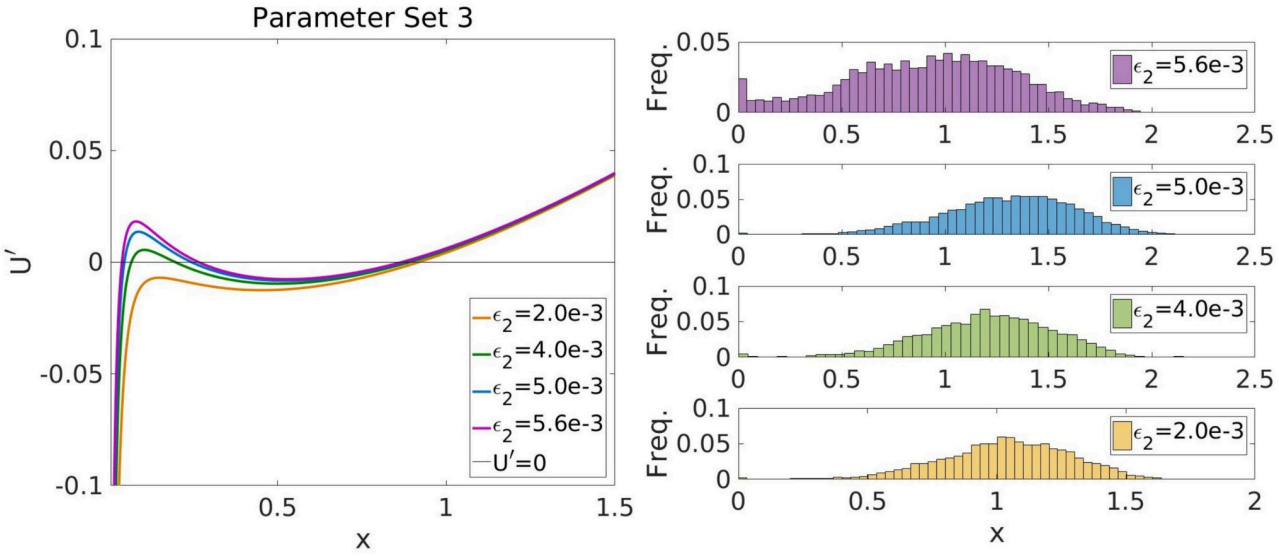

Fig 6. Noise-induced transition to bistable behaviour. This figure shows stochastic simulation results supporting the analytical prediction that our system exhibits a noise-induced transition form mono- to bi-stable behaviour. The plot shows how, as Ω decreases (i.e. the level of noise increases), the PDF of the system undergoes a transition from mono- to bi-modality.

https://doi.org/10.1371/journal.pcbi.1008408.g006

analytical approximation, noise-induced bistability ensues when the system size is reduced below its predicted critical value. Furthermore, we have ascertained that variations in ER enzyme activity induces noise-induced bistable behaviour. Fig E in S1 Text shows that modification of parameters controlling ER enzyme activity (specifically, B_2, B_8, and K_{11}) remove mean-field bistability but preserve bimodality of the PDF (i.e. bistable behaviour is noise-induced). However, noise-induced bistability remains a scarcely robust phenomenon within the bivalent TF model: the percentage of noise-induced bistable θs within the generated ensemble is $\sim$0.4% (see Table D in S1 Text) and the percentage of bistable θs that respond to parameter change by becoming noise-induced bistable barely reaches a 10% of the size of the Bistable sub-ensemble (see Fig E in S1 Text).

Tackling heterogeneity

Heterogeneity in cellular populations is one of the main obstacles regarding resistance to targeted therapies in cancer [1, 3]. Since the effects of drugs is not uniform on a heterogeneous cell population, those cells whose response is poorer become a resistant subpopulation that compromises drug efficiency. Heterogeneity has thus become a major factor in developing strategies to circumvent the emergence of resistance [84]. ER enzymes such as EZH2 have been recently proposed as targets to treat certain types of B cell leukemias [21, 83]. Since recent single-cell studies have revealed that heterogeneity also occurs in ER status [47], it is necessary to evaluate its effect on therapies that target ER enzymes.

Following [33, 34], where we put forward that heterogeneity in ER enzyme activity can be traced back to heterogeneity in the metabolic state of the cells, we analyse the effect of heterogeneity in terms of the response of the sub-ensemble of pathological θ-systems to changes in parameters that are relevant to ER enzyme activity. In this case, based on our previous discussion that allows us to identify systems within the Bistable sub-ensemble as compatible with the class of undifferentiated cells (see Fig 4k), we analyse the response of the Bistable sub-ensemble to three generic strategies: altering the activity of H3K4-modifying enzymes, altering the activity of the H3K27-modifying enzymes, and mixed strategies involving several combinations (see Fig 7c–7e, respectively). The sensitivity of the sub-ensemble to changes in parameter values, or combinations therein, is measured as the proportion of systems that become monostable (i.e. the proportion of systems that change from the Bistable into to either the High GE or the Low GE systems). Our results are shown in Fig 7 (see also Section S.1.4 in S1 Text).

We characterise heterogeneity within the (sub)ensemble using two statistics, namely, the posterior marginal PDF for each of the parameters (see Fig C in S1 Text) and the linear correlations between them. The former allows us to identify systematic, statistically significant bias in the values of each of the parameters associated with an specific behaviour (in this case, bistability) [33, 34]. In Fig 7a, we plot the $p-$value corresponding to the Kolmogorov-Smirnov (KS) test comparing the marginal PDFs of the Bistable sub-ensemble with those of the Low GE, High GE and noise-induced bimodal sub-ensembles. Provided that p is smaller than the significance level, the smaller the p-value, the more statistically significant is the difference between the marginal PDFs. Such information allows us to identify the subset of parameters which are more likely to drive the behaviour of the system from one sub-ensemble (e.g. bistable) into another (e.g. Low GE or High GE).

In order to perform our analysis, we choose the subset of parameters for which the KS test gives smaller p-values for the comparison of the Bistable sub-ensemble with the Low GE and the High GE sub-ensembles: A_3, B_2, K_2, B_8, K_8, K_{11}, and K_{12} (see Fig 7a). The motivation for such a choice is that this set of parameters are the ones that are more relevant to bistable behaviour [33, 34]. We have analysed the response of the Bistable sub-ensemble by measuring the

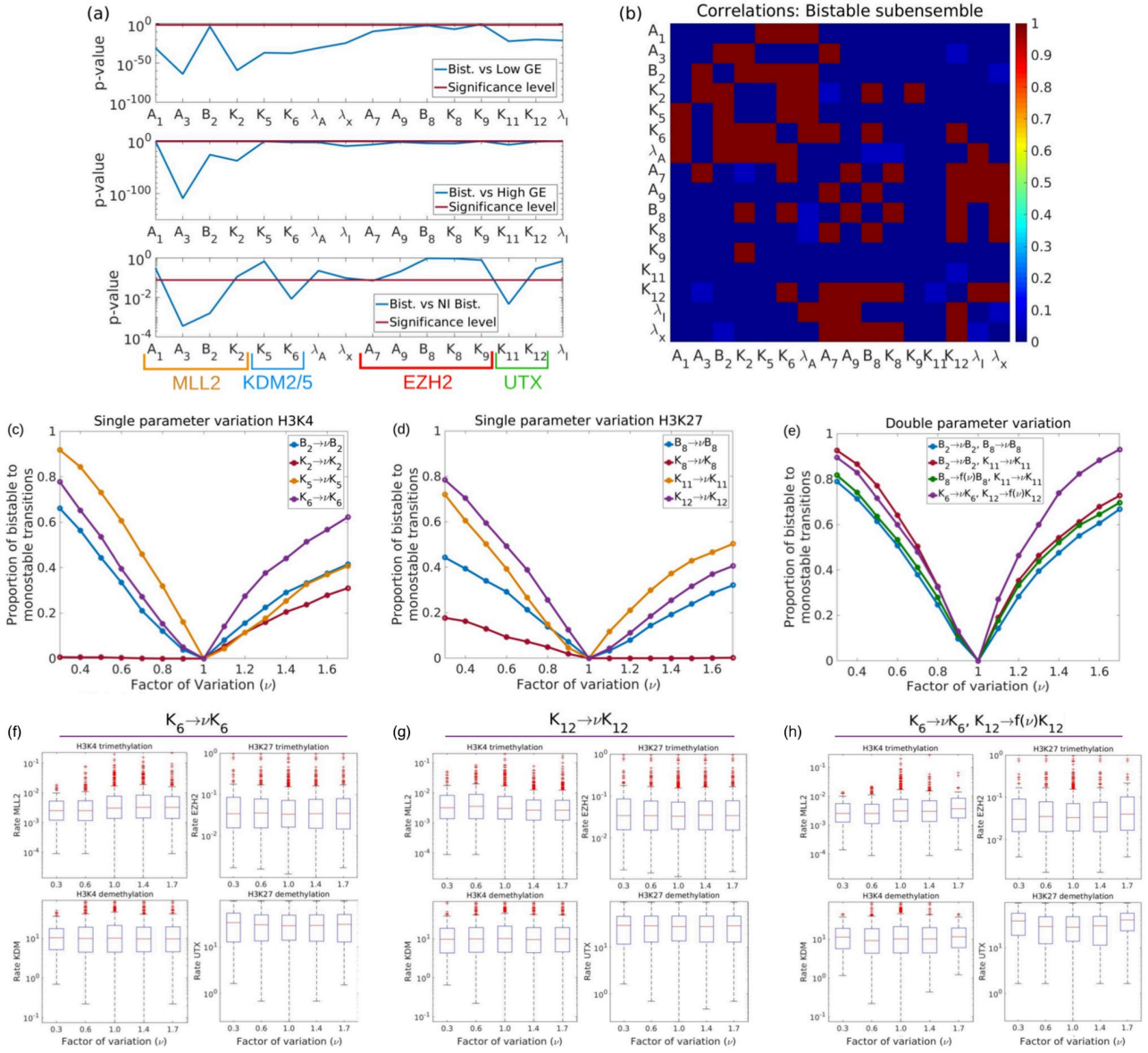

Fig 7. Tackling heterogeneity via parameter sensitivity analysis. Plot (a): p-values of the Kolmogorov-Smirnov comparison of the marginal distribution for each component of $\theta = (A_1, A_3, B_2, K_2, K_5, K_6, \lambda_A, \lambda_x, A_7, A_9, B_8, K_8, K_9, K_{11}, K_{12}, \lambda_I)$ corresponding to each of the sub-ensembles (see S1 Text, Section S.1.4.2 for details). Plot (b): correlations with the Bistable sub-ensemble. Red squares correspond to pairs such that the null hypothesis that the parameters are uncorrelated can be rejected (p-value < 0.05), dark blue, corresponds to p-values > 0.5 (uncorrelated pairs), and light blue, to p-values $\gtrsim 0.05$, i.e. pairs of parameters for which the evidence of absence of correlations is weaker. Plots (c) to (e) show the sensitivity analysis corresponding to the Bistable sub-ensemble. Recall that, according to our validation results, we are identifying the systems within this sub-ensemble with ESCs or undifferentiated cell states. Plots (c), (d), and (e) show the sensitivity to changes in kinetic parameters affecting the enzymes modifying H3K4, H3K27, and several combinations, respectively. Plots (f), (g), and (h) show the effect on the activity of chromatin modifiers under three therapeutic protocols ($K_6 \to \nu K_6$, $K_{12} \to \nu K_{12}$, and the combined $K_6 \to \nu K_6$, $K_{12} \to f(\nu)K_{12}$, respectively). Here we have defined $f(\nu) = 2 - \nu$.

https://doi.org/10.1371/journal.pcbi.1008408.g007

proportion of bistable θs that become monostable when these parameters are modified (one at a time) by a factor ν (see Fig 7d). According to such a metric, our results show that the parameters that fare better concerning their ability to beat heterogeneity are the rescaled Michaelis-Menten parameters for the KDMs (i.e. K_5 and K_6 for KDM2/KDM5 which remove me3 from trimethylated H3K4 residues and K_{11} and K_{12} for KDM6 which remove trimethyl from

H3K27me3). By contrast, our analysis shows that targeting the activity of MLL2 or EZH2 is a much poorer strategy regarding the aim of producing a maximally homogeneous sub-ensemble response.

Single parameter variations have limitations of two kinds. First, when considering $\nu > 1$, the response curve is nonlinear but very quickly saturates to a response between 35%-65%, approximately (see Fig 7c and 7d). By contrast, if $\nu < 1$, the response curve is approximately linear. Whilst this scenario is more favourable than the $\nu > 1$ one, ideally we would like to have a combination of both: a sigmoidal response curve with saturation value close to 100%. Such scenario is achieved when considering combinations of parameters (see Fig 7e). Specifically, of the combinations that we have explored, the most efficient combination is K_6-K_{12}, i.e. those involving both parameters regulating KDM activity. The reason for the enhanced efficiency of this specific combination is that K_6 and K_{12} are correlated (see Fig 7b). All other combinations that we have tried involved uncorrelated parameters and performed worse than the K_6-K_{12} one. Our result that a combination of epigenetic therapies is more efficient than the single agent ones is complementary to recent mathematical results suggesting that combinations of proliferation blockers (cytostatic drugs) and cell death enhancers (cytotoxic drugs) are more efficient at controlling drug resistance phenomena driven by cell plasticity [85, 86]. By using the characterisation of the heterogeneity in our system in terms of the activities of the chromatin modifiers, we can analyse the effect of the different epigenetic therapies in terms that are more amenable to biological interpretation and to comparison with existing results in the experimental and clinical literature. Our results can be summarised as follows.

Effects on EZH2 activity

The combinatorial therapeutic approach failed to alter the median of the activity of EZH2 (see Fig 7h) but markedly suppressed those outliers with the highest level of EZH2 activity, which remained largely unresponsive to single-targeted protocols (see Fig 7f and 7g). Therefore, although those "EZH2-high" systems with a higher biological aggressiveness [75] are more responsive to combinatorial therapy, those with lower EZH2 activity are likely to be more insidious and more difficult to clear using drugs targeting chromatin modifiers.

Effects on UTX activity

The most effective combination therapy leads to an increase in the activity of UTX (see Fig 7h). This can be better appreciated by comparing with single-target therapies, Fig 7f and 7g, in which the UTX distribution is barely affected. Such a restoration of UTX activity by efficient therapies is consistent with the role of UTX as a well-known tumour suppressor in certain cancer types [86]; however, it should be acknowledged that UTX inactivation has non-uniform effects and demands further investigation of specific outcomes in different human malignancies [87, 88].

Effects on MLL2 activity

MLL2 followed a similar pattern to that of EZH2. Thus, whereas the median activity of MLL2 was not apparently affected by either of the therapies, those "MLL2-high" outliers were the most responsive, particularly to the combined therapy.

There were no discernible patterns in the behaviour of KDM5.

Discussion

Tumor cell heterogeneity is a major barrier for efficient design of targeted anti-cancer therapies. A diverse distribution of phenotypically distinct tumour-cell subpopulations prior to drug treatment predisposes to non-uniform responses, leading to the elimination of sensitive cancer cells whilst leaving resistant subpopulations unharmed. Despite tumour cell heterogeneity has been recognized as a *bona fide* engine for drug resistance [1, 3, 84], few successful approaches [17] have been proposed aimed at formulating strategies capable of quantifying the variability associated to individual cancer cell heterogeneity and minimizing its undesirable impact on clinical outcomes. Our current work accepts this challenge to provide a computational approach that allows the rational design of combinatorial therapies involving epigenetic drugs against cancer-driving chromatin modifiers [89–91].

To analyse the effects of targeted therapies which affect the enzymatic efficiency of specific chromatin modifiers and combinations, thereupon we have formulated a stochastic model of a bivalent transcription factor [42, 43, 45, 58], for which we have been able to derive the steady-state probability distribution function *via* singular perturbation and model reduction analysis. This result allows us to characterise the different qualitative behaviours of the system (open (High GE), closed (Low GE), bistable, and noise-induced bistability). In order to tackle heterogeneity, we follow [33, 34] and generate an ensemble of models which we then classify into four sub-ensembles according to their qualitative behaviour. Comparison between analytical results and experimental data allows us to determine that the so-called Bistable and the High GE sub-ensembles show the same behaviour as undifferentiated and differentiated cell types, respectively. By contrast, the Low GE sub-ensemble failed to show any behaviour that could be identified as any cell type previously studied in [20, 21].

Since undifferentiated cells, i.e., locked in a self-renewing phenotype, have been identified as aberrant phenotypes which, if left unchecked, will eventually give rise to a tumour [21, 25, 33, 34], we have focused on analysing the role of heterogeneity within the Bistable sub-ensemble regarding their response to targeted epigenetic therapies. Such therapies are assumed to affect the value of specific parameters which alter the enzymatic activity of the corresponding chromatin modifiers and, lastly, the rate of me3 editing (addition/removal) at H3K27/K4 bivalent chromatin (Fig 8). Although our ensemble approach provided a rationale to choose those parameters to which undifferentiated (bistable) behaviour should be more sensitive [33, 34], it was not surprising that single-targeted strategies mostly failed to circumvent the therapeutic problems represented by tumour heterogeneity whereas combinatorial strategies fared much better. Specifically, those strategies involving the H3K27 and H3K4 methyltransferases EZH2 and MLL2 were predicted to be notably less effective than those involving a positive modulation of the H3K27 and H3K4 demethylating activities of KDM6A/UTX and KDM2/5.

Trithorax-like group complex containing the histone demethylases KDM6A/UTX acts antagonistically to the PRC2 complex containing the EZH2 methylase in maintaining the dynamics of the activation and repression of gene expression through H3K27 methylation. Although numerous studies have uncovered EZH2 as a useful therapeutic target using small molecule inhibitors, it has become clear that EZH2 inhibition alone may not be highly effective in certain tumors [92]. To circumvent this issue, a majority of investigators have focused on synthetic lethality approaches aimed to illuminate which tumor (sub)types harboring inactivating mutations in other epigenetic genes such as KDM6 are highly sensitive to EZH2 inhibition. Accordingly, rebalancing of H3K27me3 levels at specific genes through EZH2 inhibitors has been proposed as a therapeutic strategy in cases of multiple myeloma and urothelial bladder carcinomas harboring KDM6A/UTX mutations [93, 94]. However, although our ability to predict EZH2 sensitivity is improving, one should acknowledge that

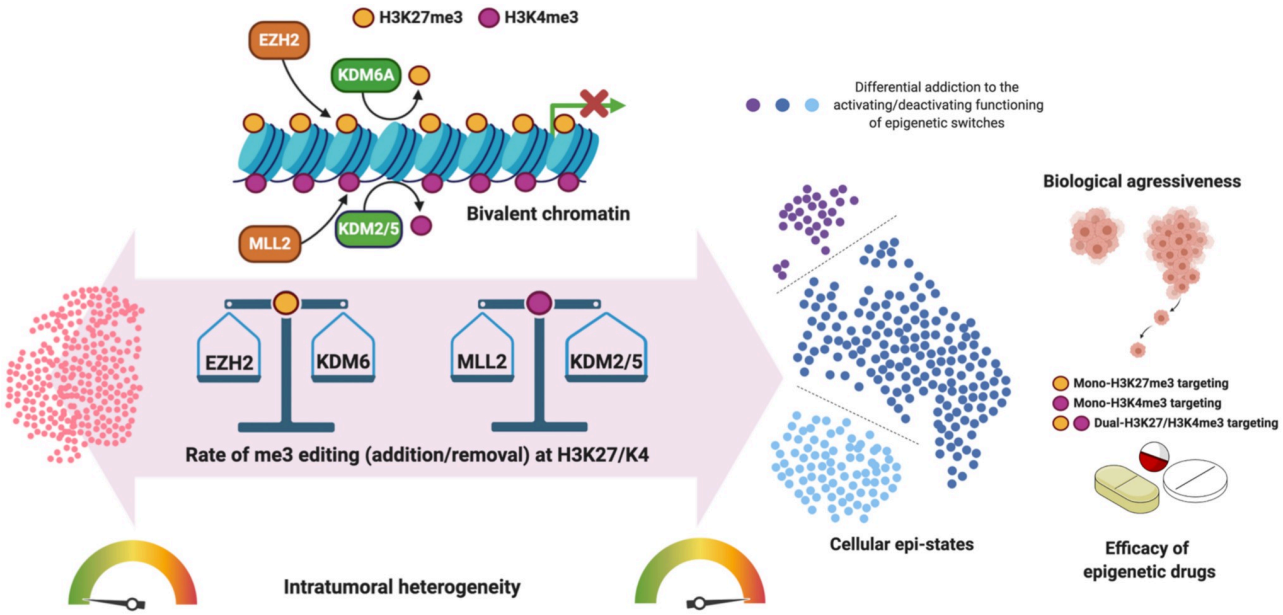

Fig 8. The heterogenous behaviour of epigenetic-regulatory systems as a determinant of the therapeutic efficacy of epigenetic drugs. The heterogenous functioning of the EZH2/KDM6A and MLL2/KDM5 switches may lead to cell-to-cell variability in terms of the addiction of cellular epi-states to certain rates of me3 editing (addition/removal) at H3K27/K4 bivalent chromatin. The proposed paradigm might accelerate future tool developments on epi-drugs applications with capability for patient stratification based on the dominant cell subtype in individual tumours. Our theoretical framework provides a coherent basis for the development of an *in silico* platform capable of identifying the epigenetic drugs combinations best-suited to therapeutically manage non-uniform responses of heterogenous cancer cell populations. Specifically, the more successful combinations involve modulators of the histone H3K4 and H3K27 demethylases KDM5 and KDM6A/UTX.

https://doi.org/10.1371/journal.pcbi.1008408.g008

more work is required to develop highly predictive biomarkers for maximizing EZH2 therapeutic benefit. Crucially, identification of non-mutational mechanisms capable of conferring EZH2 dependence to tumors could increase tumor and patient eligibility. In this regard, we now propose that stochastic dynamics of epigenetic switching suffices to dictate the emergence (and persistence) of tumor cell sub-populations with distinct degrees of responsiveness to EZH2 inhibitors in the absence of inactivating mutations of the EZH2 epigenetic partner KDM6A. Accordingly, we are accumulating evidence that transcriptional differentiation programs governed by KDM6A/UTX can enforce and safeguard cellular identity in several cancer types, thereby hindering highly aggressive cancer types by blocking epigenetic roads to de-differentiation [95–97]. On-off alterations in the normal functioning of methylating-demethylating epigenetic duos can offer therapeutic benefits beyond the EZH2/KDM6A one. Thus, inhibition of KDM5 is a valuable approach for the treatment of tumors lacking MLL2/KMT2D-regulated H3K4me3 [98] while KDM6A/UTX inhibitors can be valuable drugs in SAMRC2-deficient tumors exhibiting aberrant accumulation of H3K27me3 [99].

Our current framework, in which the intrinsic variability in the functioning of the EZH2/KDM6A and MLL2/KDM5 switches might drive the dependency of specific cancer cell types (e.g., tumor-initiating/therapy-resistant cancer stem cell-like states) on certain rates of me3 editing (addition/removal) at H3K27/K4 bivalent chromatin (Fig 8) might illuminate a purely epigenetic manner to maximize the therapeutic benefits of EZH2 and KDM inhibitors for clinical management of intratumoral heterogeneity.

Supporting information

S1 Text. Supplementary information. The file contains a more detailed description of the model formulation and model analysis, including a full derivation of the asymptotic model reduction.
(PDF)

S1 Table. Definition of the estimates or proxies for the activity of the chromatin modifiers. Statistics regarding these quantities are shown in Figs 4 and 7. Recall that $\langle f(x,z,\theta)\rangle_x = \int_0^\infty f(x,z,\theta)\phi_x(x|\theta)dx$.
(PDF)

Author Contributions

Conceptualization: Tomás Alarcón, Javier A. Menendez.

Formal analysis: Tomás Alarcón, Josep Sardanyés, Antoni Guillamon.

Investigation: Tomás Alarcón, Josep Sardanyés, Antoni Guillamon, Javier A. Menendez.

Writing – original draft: Tomás Alarcón, Josep Sardanyés, Antoni Guillamon, Javier A. Menendez.

References

1. Pisco AO, Brock A, Zhou J, Moor A, Mojtahedi M, Jackson D, et al. Non-Darwinian dynamics in therapy-induced cancer drug resistance. Nature Comm. 2013; 4:2467. https://doi.org/10.1038/ncomms3467 PMID: 24045430
2. Zhao B, Hemann MT, Lauffenburger DA. Intratumour heterogeneity alters most effective drugs in designed combinations. Proc. Natl. Acad. Sci. U.S.A. 2014; 111(29):10773–10778. https://doi.org/10.1073/pnas.1323934111
3. Chisholm RH, Lorenzi T, Lorz A, Larsen AK, de Almeida LN, Escargueil A, et al. Emergence of drug tolerance in cancer cell populations: an evolutionary outcome of selection, nongenetic instability, and stress-induced adaptation. Cancer Res. 2015; 75:930–939. https://doi.org/10.1158/0008-5472.CAN-14-2103 PMID: 25627977
4. Marusyk A, Polyak K. Tumor heterogeneity: Causes and consequences. Biochimica et Biophysica Acta (BBA)—Rev Cancer. 2010; 1805(1):105–117. https://doi.org/10.1016/j.bbcan.2009.11.002
5. Greaves M, Maley CC. Clonal evolution in cancer. Nature. 2012; 481:306–313. https://doi.org/10.1038/nature10762
6. Andor N, Graham TA, Jansen M, Xia LC, Aktipis CA, Petritcsch C, et al. Pan-cancer analysis of the extent and consequences of intratumour heterogeneity. Nat Med. 2016; 22:105–113. https://doi.org/10.1038/nm.3984 PMID: 26618723
7. Negrini S, Gorgoulis V, Halazonetis TD. Genomic instability–an evolving hallmark of cancer. Nat Rev Mol Cell Biol. 2010; 11:220–228. https://doi.org/10.1038/nrm2858
8. Brock A, Chanf H, Huang S. Non-genetic heterogeneity—a mutation-independent driving force for the somatic evolution of tumours. Nat Rev Genet. 2009; 108(20):336–342. https://doi.org/10.1038/nrg2556
9. Niepel M, Spencer SL, Sorger PK. Non-genetic cell-to-cell variability and the consequences for pharmacology. Curr Opinion Chem Biol. 2009; 13:556–561. https://doi.org/10.1016/j.cbpa.2009.09.015
10. Raj A, van Oudenaarden A. Nature, nurture, or chance: Stochastic gene expression and its consequences. Cell. 2008; 135:216–226. https://doi.org/10.1016/j.cell.2008.09.050
11. Raser JM, O'Shea EK. Noise in Gene Expression: Origins, Consequences, and Control. Science. 2005; 309:2010–2013. https://doi.org/10.1126/science.1105891
12. Biancalani T, Assaf M. Genetic toggle switch in the absence of cooperative binding: Exact results. Phys Rev Lett. 2015; 115:208101. https://doi.org/10.1103/PhysRevLett.115.208101
13. Sanchez A, Choubey S, Kondev J. Regulation of Noise in Gene Expression. Ann. Rev. Biophys. 2013; 42:469–491. https://doi.org/10.1146/annurev-biophys-083012-130401

14. Huh D, Paulsson J. Sources, propagation and consequences of stochasticity in cellular growth. Nature Genetics. 2011; 43:95–100.

15. Thomas P, Terradot G, Danos V, Weisse AY. Sources, propagation and consequences of stochasticity in cellular growth. Nat Comm. 2018; 9:4528. https://doi.org/10.1038/s41467-018-06912-9

16. Pisco AO, Huang S. Non-genetic cancer cell plasticity and therapy-induced stemness in tumour relapse: "What does not kill me strengthens me". Br J Cancer. 2015; 112:1725–1732. https://doi.org/10.1038/bjc.2015.146

17. Hayford CE, Tyson DR, Robbins CJ, Frick PL, Quaranta V, Harris LA. A unifying framework disentangles genetic, epigenetic, and stochastic sources of drug-response variability in an in vitro model of tumour heterogeneity. bioRxiv. 2020.

18. Harikumar A, Meshorer E. Chromatin remodeling and bivalent histone modifications in embryonic stem cells. EMBO reports. 2015; 16(12):1609–1619. https://doi.org/10.15252/embr.201541011

19. Blanco E, González-Ramírez M, Alcaine-Colet A, Aranda S, Croce LD. The bivalent genome: Characterization, structure, and regulation. Trends in Genetics. 2019; 35:118–131.

20. Bernstein BE, Mikkelsen TS, Xie X, Kamal M, Huebert DJ, Cuff J, et al. A bivalent chromatin structure marks key developmental genes in embryonic stem cells. Cell. 2006; 125:315. https://doi.org/10.1016/j.cell.2006.02.041 PMID: 16630819

21. Beguelin W, Popovic R, Teater M, Jiang Y, Bunting KL, Rosen M, et al. EZH2 is required for germinal center formation and somatic EZH2 mutations promote lymphoid transformation. Cancer Cell. 2013; 23:677–692. https://doi.org/10.1016/j.ccr.2013.04.011 PMID: 23680150

22. Crea F, Sun L, Mai A, Chiang YT, Farrar WL, Danesi R, et al. The emerging role of histone lysine demethylases in prostate cancer. Mol Cancer. 2012; 11:52. https://doi.org/10.1186/1476-4598-11-52 PMID: 22867098

23. Kim KH, Roberts CWM. Targeting EZH2 in cancer. Nature Medicine. 2016; 22:128–134. https://doi.org/10.1038/nm.4036

24. Plch J, Hrabeta J, Eckschlager T. KDM5 demethylases and their role in cancer cell chemoresistance. Int J Cancer. 2019; 144:221–231. https://doi.org/10.1002/ijc.31881

25. Flavahan WA, Gaskell E, Bernstein BE. Epigenetic plasticity and the hallmarks of cancer. Science. 2017; 357:eaal2380. https://doi.org/10.1126/science.aal2380

26. Mansour AA, Gafni O, Weinberger A Leeheeand Zviran, Ayyash M, Rais Y, Krupalnik V, et al. The H3K27 demethylase Utx regulates somatic and germ cell epigenetic reprogramming. Nature. 2012; 488:409–413. https://doi.org/10.1038/nature11272 PMID: 22801502

27. Menéndez JA, Corominas-Faja B, Cuyàs E, García MG, Fernández-Arroyo S, Fernández AF, et al. Oncometabolic nuclear reprogramming of cancer stemness. Stem Cell Reports. 2016; 6:273–283. https://doi.org/10.1016/j.stemcr.2015.12.012 PMID: 26876667

28. Waddington CH. Canalisation of development and the inheritance of acquired characters. Nature. 1942; 150:563–565. https://doi.org/10.1038/150563a0

29. Hilfinger A, Paulsson J. Separating intrinsic from extrinsic fluctuations in dynamic biological systems. Proc. Natl. Acad. Sci. U.S.A. 2011; 108:12167–12172. https://doi.org/10.1073/pnas.1018832108

30. Singh A, Soltani M. Quantifying Intrinsic and Extrinsic Variability in Stochastic Gene Expression Models. PLOS ONE. 2014; p. 1–12.

31. Wang J, Zhang K, Xu L, Wang E. Quantifying the Waddington landscape and biological paths for development and differentiation. Proc. Natl. Acad. Sci. U.S.A. 2011; 108(20):8257–8262. https://doi.org/10.1073/pnas.1017017108

32. Tse M, Chu B, Roy M, Read E. DNA-Binding Kinetics Determines the Mechanism of Noise-Induced Switching in Gene Networks. Biophysical Journal. 2015; 109(8):1746–1757. https://doi.org/10.1016/j.bpj.2015.08.035

33. Folguera-Blasco N, Cuyàs E, Menéndez JA, Alarcón T. Epigenetic regulation of cell fate reprogramming in aging and disease: A predictive computational model. PLoS Comp Biol. 2018; 14:e1006052. https://doi.org/10.1371/journal.pcbi.1006052

34. Folguera-Blasco N, Pérez-Carrasco R, Cuyás E, Menéndez JA, Alarcón T. A multiscale model of epigenetic heterogeneity reveals the kinetic routes of pathological cell fate reprogramming. PLoS Comp Biol. 2019; 15:e1006592. https://doi.org/10.1371/journal.pcbi.1006592

35. Wagner A. Robustness and evolvability in living systems. Princeton University Press, Princeton, NJ, U.S.A; 2007.

36. Wagner A. Neutralism and selectionism: A network-based reconciliation. Nature Rev Genetics. 2008; 9:965–974. https://doi.org/10.1038/nrg2473

37. Aguirre J, Buldú JM, Stich M, Manrubia SC. Topological sturcture of the space of phneotypes: The case of RNA neutral networks. PLoS One. 2011; 6:e26324. https://doi.org/10.1371/annotation/fb422230-9702-4eed-ad96-1c4cd2ab5e5d

38. Wagner A. The role of robustness in phenotypic adaptation and innovation. Proc Roy Soc B. 2012; 279:1249–1258. https://doi.org/10.1098/rspb.2011.2293

39. Ibáñez-Marcelo E, Alarcón T. The topology of robustness and evolvability in evolutionary systems with genotype-phenotype map. J Theor Biol. 2014; 356:144–162. https://doi.org/10.1016/j.jtbi.2014.04.014

40. Yubero P, Manrubia S, Aguirre J. The space of genotypes is a network of networks: implications for evolutionary and extinction dynamics. Sci Rep. 2017; p. 13813. https://doi.org/10.1038/s41598-017-14048-x

41. Sneppen K, Michelson MA, Dodd IB. Ultrasensitive gene regulation by positive feedback loops in nucleosome modification. Molecular Systems Biology. 2008; 4:182. https://doi.org/10.1038/msb.2008.21

42. Thalheim T, Herberg M, Loeffler M, Galle J. The Regulatory Capacity of Bivalent Genes 014A Theoretical Approach. Int J Molec Sci. 2017; 18(5):1069. https://doi.org/10.3390/ijms18051069

43. Thalheim T, Hopp L, Binder H, Aust G, Galle J. On the Cooperation between Epigenetics and Transcription Factor Networks in the Specification of Tissue Stem Cells. Epigenomes. 2018; 2(4):20. https://doi.org/10.3390/epigenomes2040020

44. Schvartzman JM, Thomson CB, Finley LWS. Metabolic regulation of chromatin modifications and gene expression. J Cell Biol. 2018; 7:2247–2259. https://doi.org/10.1083/jcb.201803061

45. Zhang Y, Liu N, Lin W, Li C. Quantifying the interplay between genetic and epigenetic regulations in stem cell development. N J Phys. 2019; 21(10):103042. https://doi.org/10.1088/1367-2630/ab4c82

46. Pour M, Pilzer I, Rosner R, Smith ZD, Meissner A, Nachman I. Epigenetic predisposition to reprogramming fates. EMBO Reports. 2015; 18:370–378. https://doi.org/10.15252/embr.201439264

47. Rotem A, Ram O, Shoresh N, Sperling RA, Goren A, Weitz DA, et al. Single-cell ChIP-seq reveals cell subpopulations defined by chromatin state. Nature Biotechnology. 2015; 33:1165. https://doi.org/10.1038/nbt.3383 PMID: 26458175

48. Bintu L, Young J, Antebi YE, McCue K, Kazuki Y, Uno N, et al. Dynamics of epigenetic regulation at the single-cell level. Science. 2016; 351:720–724. https://doi.org/10.1126/science.aab2956 PMID: 26912859

49. Cortini R, Barbi M, Care BR, Lavelle C, Lesne A, Mozziconacci J, et al. The physics of epigenetics. Rev Mod Phys. 2016; 88:025002. https://doi.org/10.1103/RevModPhys.88.025002

50. Gillespie DT. A general method for numerically simulating the stochastic time evolution of coupled chemical reactions. J Comp Phys. 1976; 22:403–434. https://doi.org/10.1016/0021-9991(76)90041-3

51. Gillespie DT. Exact stochastic simulation of coupled chemical reactions. J Phys Chem. 1977; 81:2340–2361. https://doi.org/10.1021/j100540a008

52. Ringrose L, Howard M. Dissecting chromatin-mediated gene regulation and epigenetic memory through mathematical modelling. Curr Opinion Syst Biol. 2017; 3:7–14. https://doi.org/10.1016/j.coisb.2017.02.003

53. Tian XJ, Zhang H, Sannerud J, Xing J. Achieving diverse and monoallelic olfactory receptor selection through dual-objective optimization design. Proc. Natl. Acad. Sci. U.S.A. 2016; 113:E2889–E2898. https://doi.org/10.1073/pnas.1601722113

54. Dodd IB, Micheelsen MA, Sneppen K, Thon G. Theoretical analysis of epigenetic cell memory by nucleosome modification. Cell. 2007; 129:813–822. https://doi.org/10.1016/j.cell.2007.02.053

55. David-Rus D, Mukhopadhyway S, Lebowitz JL, Sengupta AM. Inheritance of epigenetic chormatin silencing. J Theor Biol. 2009; 258:112–120. https://doi.org/10.1016/j.jtbi.2008.12.021

56. Sneppen K, Dodd IB. A simple histone code opens many paths to epigenetics. PLoS Comp Biol. 2012; 8:e1002643. https://doi.org/10.1371/journal.pcbi.1002643

57. Sneppen K, Dodd IB. Nucleosome dynamics and maintenance of epigenetic states of CpG islands. Phys Rev E. 2016; 93:062417. https://doi.org/10.1103/PhysRevE.93.062417

58. Sneppen K, Ringrose L. Theoretical analysis of Polycomb-Trithorax systems predicts that poised chromatin is bistable and not bivalent. Nature Comm. 2019; 10:2133. https://doi.org/10.1038/s41467-019-10130-2

59. Samoilov M, Plyasunov S, Arkin AP. Stochastic amplification and signaling in enzymatic futile cycles through noise-induced bistability with oscillations. Proc. Natl. Acad. Sci. U.S.A. 2005; 102:2310–2315. https://doi.org/10.1073/pnas.0406841102

60. Frigola D, Casanellas L, Sancho JM, Ibañes M. Asymmetric stochastic switching driven by intrinsic molecular noise. PLoS One. 2012; 7:e31407. https://doi.org/10.1371/journal.pone.0031407

61. Pujadas E, Feinberg A. Regulated Noise in the Epigenetic Landscape of Development and Disease. Cell. 2012; 148(6):1123–1131. https://doi.org/10.1016/j.cell.2012.02.045

62. Weber M, Buceta J. Stochastic stablisation of phenotypic states: the genetrric bistable switch as a case study. PLoS One. 2013; 8:e73487. https://doi.org/10.1371/journal.pone.0073487

63. Aquino G, Rocco A. Bimodality without feedback: Noise-induced transitions in the repressed gene with extrinsic log-normal noise; 2019.

64. Horsthemke W, Lefever R. Noise-induced transitions. Springer-Verlag, New York, NY, USA; 2006.

65. Sneeringer CJ, Scott MP, Kuntz KW, Knutson SK, Pollock RM, Richon VM, et al. Coordinated activities of wild-type plus mutant EZH2 drive tumour-associated hypertrimethylation of lysine 27 on histone H3 (H3K27) in human B-cell lymphomas. Proc. Natl. Acad. Sci. U.S.A. 2010; 107(49): 20980–20985. https://doi.org/10.1073/pnas.1012525107 PMID: 21078963

66. Keener J, Sneyd J. Mathematical physiology. Springer-Verlag, New York, NY, USA; 1998.

67. Rotili D, Mai A. Targeting Histone Demethylases: A New Avenue for the Figureht against Cancer. Genes & Cancer. 2011; 2(6):663–679. https://doi.org/10.1177/1947601911417976

68. Shpargel KB, Starmer J, Yee D, Pohlers M, Magnuson T. KDM6 Demethylase Independent Loss of Histone H3 Lysine 27 Trimethylation during Early Embryonic Development. PLOS Genetics. 2014; 10 (8):1–16. https://doi.org/10.1371/journal.pgen.1004507

69. Ingalls BP. Mathematical modelling in systems biology. An introduction. The MIT Press, Cambridge, Massachusets, USA; 2013.

70. Gardiner CW. Stochatic methods. Springer-Verlag, Berlin, Germany; 2009.

71. Bressloff PC. Stochastic processes in cell biology. Springer-Verlag, Berlin, Germany.; 2014.

72. Bruna M, Chapman SJ, Smith MJ. Model reduction for slow-fast stochastic systems with metastable behaviour. J Chem Phys. 2014; 140:174107. https://doi.org/10.1063/1.4871694

73. Ward MJ. Exponential asymptotics and convection-reaction-diffusion models. In: Cronin J, O'Mailley RE, editors. Analysing multiscale phenomena using singular perturbation methods. Providence, RI, USA: American Mathematical Society; 1999. p. 162–195.

74. Mas G, Blanco E, Ballaré C, Sansó M, Spill YG, Hu D, et al. Promoter bivalency favors an open chromatin architecture in embryonic stem cells. Nature Genetics. 2018; 50:1452–1462. https://doi.org/10.1038/s41588-018-0218-5 PMID: 30224650

75. Chang JW, Gwak SY, Shim G-A, Liu L, Lim YC, Kim JM et al. EZH2 is associated with poor prognosis in head-and-neck squamous cell carcinoma via regulating the epithelial-to-mesenchymal transition and chemosensitivity Oral Oncol. 2016; 52:66–74. https://doi.org/10.1016/j.oraloncology.2015.11.002 PMID: 26604082

76. Yamagishi M, Uchimaru K. Targeting EZH2 in cancer therapy Curr. Opin. Oncol. 2017; 39:375–381. https://doi.org/10.1097/CCO.0000000000000390

77. Jones BA, Varambally S, Arend RC. Histone Methyltransferase EZH2: A Therapeutic Target for Ovarian Cancer Mol Cancer Ther. 2018; 17:591–602. https://doi.org/10.1158/1535-7163.MCT-17-0437

78. Duan R, Du W, Guo W. EZH2: a novel target for cancer treatment J Hematol Oncol. 2020; 13:104. https://doi.org/10.1186/s13045-020-00937-8

79. Kang N, Eccleston M, Clermont P-L, Latarani M, Male DK, Wang Y, et al. EZH2 inhibition: a promising strategy to prevent cancer immune editing Epigenomics. 2020; 12:1457–1476. https://doi.org/10.2217/epi-2020-0186 PMID: 32938196

80. Zhang J, Dominguez-Sola D, Hussein S, Lee J-E, Holmes AB, Bansal M, et al. Disruption of KMT2D perturbs germinal center B cell development and promotes lymphomagenesis Nature Medicine 2015; 21:1190–1198. https://doi.org/10.1038/nm.3940 PMID: 26366712

81. Ardeshir-Larijani F, Bhateja P, Lipka MB, Sharma N, Fu P, Dowlati A. KMT2D mutation is associated with poor prognosis in non–small-cell lung cancer Clinical Lung Cancer. 2018; 19:E489–E501. https://doi.org/10.1016/j.cllc.2018.03.005

82. Rabello D, Ferreira V, Berzoti-Coelho MG, Burin SM, Magro CL, Cacemiro M, et al. MLL2/KMT2D and MLL3/KMT2C expression correlates with disease progression and response to imatinib mesylate in chronic myeloid leukemia Cancer Cell Int. 2018; 18:26 https://doi.org/10.1186/s12935-018-0523-1 PMID: 29483845

83. Beguelin W, Rivas MA, Calvo-Fernandez MT, Teater M, Puwarda A, Redmond D, et al. EZH2 enables germinal centre formation through epigenetic silencing of CDKN1A and an Rb-E2F1 feedback loop. Nature Comm. 2017; 8:877. https://doi.org/10.1038/s41467-017-01029-x

84. Dagogo-Jack I, Shaw AT. Tumour heterogeneity and resistance to cancer therapies. Nature Reviews Clinical Oncological. 2018; 15:81–94. https://doi.org/10.1038/nrclinonc.2017.166

85. Lorz A, Lorenzi T, Hochberg ME, Clairambault J, Perthame B. Populational adaptive evolution, chemotherapeutic resistance and multiple anti-cancer therapies ESAIM: M2AN. 2013; 47:377–399. https://doi.org/10.1051/m2an/2012031

86. Stace REA, Stiehl T, Chaplain MAJ, Marciniak-Czochra A, Lorenzi T Discrete and continuum phenotype-structured models for the evolution of cancer cell populations under chemotherapy. Math. Model. Nat. Phenom. 2020; 15:14. https://doi.org/10.1051/mmnp/2019027

87. Jiang H. The expanding vulnerabilities of being UTXless. Sig. Transduct. Target. Ther. 2019; 4:12. https://doi.org/10.1038/s41392-019-0043-z

88. Schulz WA, Lang A, Koch J, Greife A. The histone demethylase UTX/KDM6A in cancer: Progress and puzzles. Int. J. Cancer. 2019; 145:614–620. https://doi.org/10.1002/ijc.32116

89. Cai SF, Chen CW, Armstrong SA. Drugging Chromatin in Cancer: Recent Advances and Novel Approaches. Mol Cell. 2015; 60:561–570. https://doi.org/10.1016/j.molcel.2015.10.042

90. Baskin NL, Haynes KA. Chromatin engineering offers an opportunity to advance epigenetic cancer therapy. Nature Structural & Molecular Biology. 2019; 26:842–845. https://doi.org/10.1038/s41594-019-0299-6

91. Patnaik S, Anupriya A. Drugs Targeting Epigenetic Modifications and Plausible Therapeutic Strategies Against Colorectal Cancer. Front Pharma. 2019; 10:588. https://doi.org/10.3389/fphar.2019.00588

92. Eich ML, Athar M, Ferguson JE 3rd, Varambally S. EZH2-Targeted Therapies in Cancer: Hype or a Reality. Cancer Res. 2020; 80:5449–5458. https://doi.org/10.1158/0008-5472.CAN-20-2147

93. Ler LD, Ghosh S, Chai X, Thike AA, Heng HL, Siew EY, et al. Loss of tumor suppressor KDM6A amplifies PRC2-regulated transcriptional repression in bladder cancer and can be targeted through inhibition of EZH2. Sci Transl Med. 2017; 9:eaai8312. https://doi.org/10.1126/scitranslmed.aai8312 PMID: 28228601

94. Ezponda T, Dupere-Richer D, Will CM, Small EC, Varghese N, Patel T, et al. UTX/KDM6A Loss Enhances the Malignant Phenotype of Multiple Myeloma and Sensitizes Cells to EZH2 inhibition. Cell Rep. 2017; 21:628–640. https://doi.org/10.1016/j.celrep.2017.09.078 PMID: 29045832

95. Taube JH, Sphyris N, Johnson KS, Reisenauer KN, Nesbit TA, Joseph R, et al. The H3K27me3-demethylase KDM6A is suppressed in breast cancer stem-like cells, and enables the resolution of bivalency during the mesenchymal-epithelial transition. Oncotarget. 2017; 8:65548–65565. https://doi.org/10.18632/oncotarget.19214 PMID: 29029452

96. Andricovich J, Perkail S, Kai Y, Casasanta N, Peng W, Tzatsos A. Loss of KDM6A Activates Super-Enhancers to Induce Gender-Specific Squamous-like Pancreatic Cancer and Confers Sensitivity to BET Inhibitors. Cancer Cell. 2018; 33:512–526.e8. https://doi.org/10.1016/j.ccell.2018.02.003

97. Kalisz M, Bernardo E, Beucher A, Maestro MA, Del Pozo N, Millán I, et al. HNF1A recruits KDM6A to activate differentiated acinar cell programs that suppress pancreatic cancer. EMBO J. 2020; 39: e102808. https://doi.org/10.15252/embj.2019102808 PMID: 32154941

98. Heward JA, Konali L, D'Avola A, Close K, Yeomans A, Philpott M, et al. KDM5 inhibition offers a novel therapeutic strategy for the treatment of KMT2D mutant lymphomas. bioRxiv 2020.06.30.177477. https://doi.org/10.1101/2020.06.30.177477. PMID: 33786580

99. Romero OA, Vilarrubi A, Alburquerque-Bejar JJ, Gomez A, Andrades A, Trastulli D, et al. SMARC4 deficient tumours are vulnerable to KMD6A/UTX and KDM6B/JMJD3 blockade. bioRxiv 2020.08.07.241232; https://doi.org/10.1101/2020.08.07.241232.